

See discussions, stats, and author profiles for this publication at: <https://www.researchgate.net/publication/263586241>

Photoisomerization Dynamics and Pathways of Trans- and Cis-Azobenzene in Solution from Broadband Femtosecond Spectroscopies and Calculations.

ARTICLE *in* THE JOURNAL OF PHYSICAL CHEMISTRY B · JULY 2014

Impact Factor: 3.3 · DOI: 10.1021/jp504999f · Source: PubMed

CITATIONS

9

READS

29

10 AUTHORS, INCLUDING:



A. L. Dobryakov

Humboldt-Universität zu Berlin

72 PUBLICATIONS 855 CITATIONS

[SEE PROFILE](#)



Mario Gerecke

Humboldt-Universität zu Berlin

5 PUBLICATIONS 17 CITATIONS

[SEE PROFILE](#)



Alexander A. Granovsky

Kintech Lab

79 PUBLICATIONS 639 CITATIONS

[SEE PROFILE](#)



Sergey A Kovalenko

Humboldt-Universität zu Berlin

153 PUBLICATIONS 2,816 CITATIONS

[SEE PROFILE](#)

Photoisomerization Dynamics and Pathways of *trans*- and *cis*-Azobenzene in Solution from Broadband Femtosecond Spectroscopies and Calculations

M. Quick,[†] A. L. Dobryakov,[†] M. Gerecke,[†] C. Richter,[†] F. Berndt,[†] I. N. Ioffe,[‡] A. A. Granovsky,[§] R. Mahrwald,[†] N. P. Ernsting,^{*,†} and S. A. Kovalenko^{*,†}

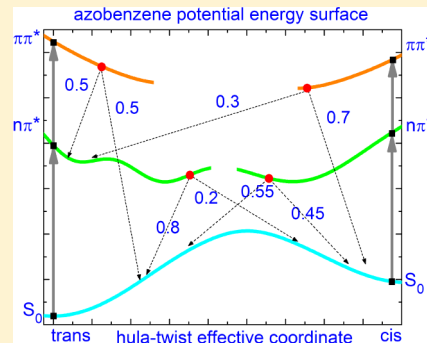
[†]Department of Chemistry, Humboldt-Universität zu Berlin, Brook-Taylor-Str. 2, D-12489 Berlin, Germany

[‡]Department of Chemistry, Lomonosov Moscow State University, 119991 Moscow, Russia

[§]Firefly Project, Moscow 117593, Russia

Supporting Information

ABSTRACT: The photoisomerization of azobenzene in solution was studied experimentally and by calculations. *trans*-to-*cis* and *cis*-to-*trans* dynamics are described through broadband transient absorption, fluorescence, and stimulated Raman spectroscopy. Transient absorption was extended to cover not only the $n\pi^*$ band but also the $\pi\pi^*$ band in the ultraviolet. Isomerization yields are used for a quantitative comparison of *trans* and *cis* transient spectra under different excitation. For the *trans*-to-*cis* path upon $n\pi^*(S_1)$ excitation, the evolution develops with 0.3, 3, and 16 ps. The first two times reflect population relaxation to a local minimum S_{1t}^L and subsequent transition to a dark intermediate S_{1t}^D over an 8 kJ/mol barrier. The existence of stationary points S_{1t}^L and S_{1t}^D is confirmed by quantum-chemical calculations. The third time corresponds to $S_{1t}^D \rightarrow S_0$ relaxation to the ground state via an S_1/S_0 conical intersection over a 12 kJ/mol barrier. Thus, the 16 ps time constant is attributed to the isomerization process and not to vibrational cooling, contrary to the current view and in line with the previous interpretation by Lednev et al. (*J. Phys. Chem.* **1996**, *100*, 13338). The decay of the long-lived intermediate S_{1t}^D is consistent with the hula twist rather than with the inversion mechanism. For the *cis*-to-*trans* reaction following $n\pi^*$ excitation, signal decay is strongly nonexponential, with 0.1 and 1 ps. The latter (1 ps) is much shorter than the 16 ps decay of the *trans* isomer, implying different S_1/S_0 conical intersections and relaxation paths for the *cis*-to-*trans* and *trans*-to-*cis* reaction. New results are also obtained with $\pi\pi^*(S_n)$ excitation. Thus, for *trans*-azobenzene, 50% of the population relaxes to an S_1 region, which is not accessible under $n\pi^*$ excitation. For *cis*-azobenzene, up to 30% of the excited species isomerize to *trans* via an S_n/S_1 intersection, resulting in a mixed *cis*/*trans* S_1 population. The isomerization kinetics of azobenzene shows no viscosity dependence, putting into question the torsion mechanism and suggesting the hula-twist isomerization mechanism.



1. INTRODUCTION

Azobenzene^{1–4} and stilbene^{5–7} are well-known photoswitches, which isomerize under the action of light. Despite similarities in the molecular structure of these compounds, their isomerization properties differ in important aspects. Azobenzene is capable of isomerization under strong constraints,^{1–4,8–12} for example, in the tight environment of solid matrices or when included in a polymer chain, which has never been observed for stilbene. This unique feature of azobenzene led to its prominence in the development of new materials with light-driven properties.^{8–10}

Feasible isomerization paths are sketched in Scheme 1. The first and most apparent one corresponds to torsion about the central double bond. Next comes inversion at a nitrogen center as the phenyl rings move toward each other in the molecular plane. This path is not active in stilbene because its ethylenic hydrogens prevent such a transformation. The third is the hula-twist,^{11–17} which is essentially multidimensional and represents

a pedal-like^{11,12} concerted motion of the nitrogens and phenyls. Here the C_1NN' plane rotates by 180° about an instantaneous axis through atoms C_1 and N' , with the phenyls approaching each other nearly in the molecular plane, similar to inversion. Interestingly, this pathway is, in principle, also allowed for stilbene. One of the aims of the present work is to examine which path is actually realized.

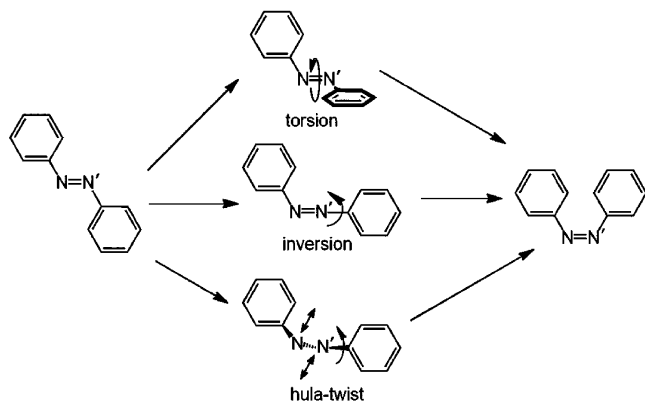
Azobenzene absorption spectra are displayed in Figure 1. They show an intense $\pi\pi^*$ band peaked at 316 nm and a weak $n\pi^*$ band around 440 nm. For stilbene, only the $\pi\pi^*$ band exists while $n\pi^*$ is absent. This results in dramatic differences in photochemistry and spectroscopy of the compounds. When excited to $\pi\pi^*(S_n)$ or $n\pi^*(S_1)$, *trans*-azobenzene has different isomerization yields, in violation of Kasha's rule.^{18,19} We note in

Received: May 21, 2014

Revised: June 30, 2014

Published: July 1, 2014



Scheme 1^a

^aIsomerization pathways of azobenzene: Torsion about the central double bond (top); inversion (middle) when the phenyl rings move towards each other in the molecular plane; and hula-twist (bottom) representing a pedal-like concerted motion of the nitrogens and phenyls. Here the C₁NN' plane angle rotates about the instantaneous C₁N' axis by 180° with the phenyls approaching each other similar to the inversion mechanism.

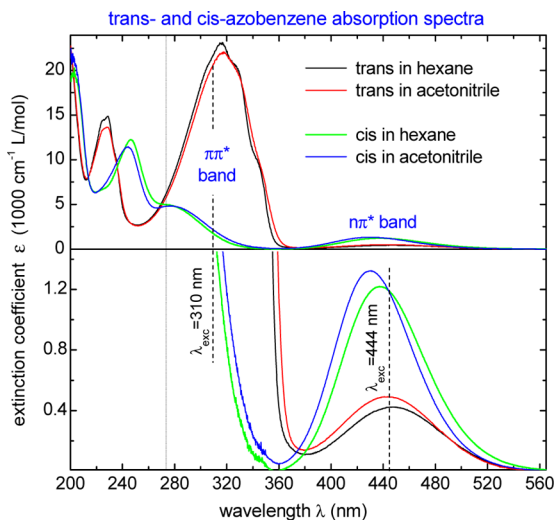


Figure 1. *trans*-Azobenzene $A_t(\lambda)$ and *cis*-azobenzene $A_c(\lambda)$ absorption spectra in acetonitrile and *n*-hexane. Excitation wavelength in TA measurements was $\lambda_{\text{exc}} = 310$ or 444 nm; the shortest TA probe wavelength was 275 nm.

passing that transient absorption (TA) experiments are complicated due to the weak $n\pi^*$ transition. Although highly concentrated samples may provide sufficient $n\pi^*$ absorbance, under these conditions the $\pi\pi^*$ band cannot be observed because its absorbance becomes too high. At the same time with low sample concentrations, transient signals are small and difficult to record.

In the 1980s, Rau^{1–3} measured isomerization yields of sterically hindered azobenzenes and found the yields to be identical upon $n\pi^*$ and $\pi\pi^*$ excitation, unlike for parent azobenzene, where they differ by a factor 2. To explain these observations, he proposed that upon $n\pi^*$ excitation *trans*-azobenzene isomerizes via inversion, while upon $\pi\pi^*$ excitation also a torsional reaction channel becomes active. The latter would be blocked in the sterically hindered compound, resulting in equal $n\pi^*$ and $\pi\pi^*$ isomerization yields. This

interpretation has been used in most of the experimental studies discussed below.

A few transient studies^{20–31} were performed in 1996–2005. Lednev et al.^{20–22} investigated TA kinetics of *trans*-azobenzene upon $\pi\pi^*(S_n)$ excitation. Triexponential decay with 0.2, 1, and 13 ps was ascribed, respectively, to $S_n \rightarrow S_1$ relaxation, formation of a “bottleneck” S_1 state, and $S_1 \rightarrow S_0$ internal conversion. The characteristic times were generally confirmed and measured more precisely by other groups.^{23–31} Zinth and coworkers^{23–25} applied broadband TA to *trans* and *cis* isomers upon $n\pi^*$ excitation. They found 0.3, 2.6, and 12 ps decays for *trans*- and faster ones, 0.1 and 1 ps, for *cis*-azobenzene.^{23,24} Similar time constants were also obtained with $\pi\pi^*$ excitation.²⁵ However, the interpretation of experimental data in these and other studies^{23–28} was changed dramatically. Namely, $\tau_1 = 0.3$ ps was associated with the population escape from the Franck–Condon region, $\tau_2 = 2.6$ ps was attributed to the $S_1 \rightarrow S_0$ relaxation to the ground state, and $\tau_3 = 12$ ps was ascribed to vibrational cooling in S_0 . This view of the excited-state evolution has become common, as is reflected in a recent review.³²

Additional features were reported by Tahara and coworkers^{27,28} from time-resolved Raman and fluorescence studies of *trans*-azobenzene under $\pi\pi^*$ excitation. The $S_n \rightarrow S_1$ relaxation time was reported to be 0.11 ps. Furthermore, fluorescence yields from the S_n and S_1 states were estimated to be nearly identical. It was concluded that no isomerization occurs in S_n or during $S_n \rightarrow S_1$ relaxation. The authors also recorded Raman S_1 and S_0 spectra of *trans*-azobenzene and found them to be very similar.²⁸ On the basis of this similarity, they excluded S_1 torsion and proposed inversion for the isomerization mechanism.

Interesting results were obtained by transient fluorescence spectroscopy. Temps and coworkers³⁰ measured *trans*-azobenzene and its capped (sterically hindered) analogue under $n\pi^*$ excitation. For both compounds, very close relaxation kinetics were reported, indicating either the inversion or the hula-twist isomerization pathway. Diau and coworkers³¹ studied the fluorescence anisotropy of *trans*-azobenzene in solvents of different viscosities. Fast anisotropy decay was observed in *n*-hexane but not in ethylene glycol. The authors concluded that the isomerization proceeds via torsion in low viscous liquids and via inversion in highly viscous ones.

Numerous quantum-chemical calculations^{1,11–17,33–40} were performed to clarify the isomerization pathways of azobenzene. Up to now, many workers have considered torsion^{35–40} to be the most probable mechanism, although the hula-twist may provide a better explanation.^{11–17}

In the present paper, we reexamine the photoinduced excited-state dynamics of *trans*- and *cis*-azobenzene with broadband transient absorption, fluorescence, and Raman spectroscopies. TA spectroscopy is extended to the ultraviolet region, where the complete evolution of the $\pi\pi^*$ bleach band is observed. This allows us to evaluate directly the contribution of vibrational cooling in the decay kinetics. We also use the isomerization yields to normalize transient spectra to a given population for a precise comparison of *trans* and *cis* spectra under different excitations. This leads to a reinterpretation of the excited-state evolution and a reassessment of isomerization pathways. We also report first transient fluorescence spectra of *trans*-azobenzene and stimulated Raman spectra in the S_0 , S_1 , and S_n states.

2. EXPERIMENT AND CALCULATIONS

2.1. Compounds, Thermal cis-to-trans Isomerization in the Dark. *trans*-Azobenzene (99%, Acros Organics) was measured without further purification. The *cis* isomer was obtained photochemically by illuminating a *n*-hexane solution of *trans*-azobenzene with a mercury lamp in the range 275–375 nm (filter FGUV11, Thorlabs). About 0.5 g of *cis* was produced within an hour then chromatographically purified (99%) and finally kept in the crystalline phase at –20 °C. Sample purity was checked by absorption spectra. (An example is in Figure 1.) No change in *cis* absorption was found upon 4 months of storage in the fridge. Thermal (dark) *cis*-to-*trans* isomerization in *n*-hexane was measured to occur with 200 and 20 h at 20 and 40 °C, respectively. (See Figure S1 in Supporting Information (SI).)⁶² The S_0 *cis*-to-*trans* isomerization barrier is estimated as 87.9 kJ/mol.

2.2. Transient Absorption Measurements. The TA setup with applications were described elsewhere.^{41–48} The setup provides spectral coverage 275–690 nm with a 0.1 ps instrument response and timing precision of 0.02 ps over the full probe range. Multiple (10–20) pump–probe scans were performed to improve the signal-to-noise. TA spectra $\Delta A(\lambda, t)$ were recorded at the magic angle and for parallel $\Delta A_{\parallel}(\lambda, t)$ and perpendicular $\Delta A_{\perp}(\lambda, t)$ pump–probe polarization. Transient anisotropy is calculated as

$$\begin{aligned}\rho(\lambda, t) &= (\Delta A_{\parallel} - \Delta A_{\perp}) / (\Delta A_{\parallel} + 2\Delta A_{\perp}) \\ &= (\Delta A_{\parallel} - \Delta A_{\perp}) / (3\Delta A)\end{aligned}\quad (1)$$

A 30 mL solution of 0.5 mg/mL of *trans* or 1.4 mg/mL of *cis* was flown through a sample cell of 0.3 mm internal thickness. The absorbance $A(\lambda)$ at 315 nm was <0.6 for $\pi\pi^*$ excitation and <0.9 for $n\pi^*$ excitation. The pump and probe beams were focused onto the cell at 15° to 0.1 mm spots.

2.3. Transient Fluorescence. Time-resolved fluorescence spectra of *trans*-azobenzene in *n*-hexane were recorded upon 400 nm ($n\pi^*$) excitation (at 500 Hz repetition rate) with our broadband upconversion setup.^{49–51} The sample thickness was 0.4 mm in a flow cell with 1.6 optical density at 400 nm. To reduce scattering the fluorescence signal $I_{\perp}(\lambda, t)$ was recorded with perpendicular pump–probe polarization. Upconverted fluorescence, generated in a 0.5 mm BBO crystal with tilted gate pulses at 1345 nm, was dispersed in a spectrograph and registered on a CCD camera (Andor DV 420-BU). The pump–probe cross-correlation was 0.2 ps (fwhm). Time-resolved spectra integrated over 3 s were recorded with 0.02, 0.1, or 1 ps steps. The upconverted signal was 9 to 10 counts/pixel in the fluorescence peak. Transient spectra were averaged over 16 scans, time-corrected, and fitted with log-normal functions.

2.4. Femtosecond Stimulated Raman. The transient Raman setup^{52–54} was generally similar to that for TA. The picosecond, spectrally narrow (10 cm^{-1}) Raman pump (0.2 μJ , 920 Hz) was tuned to $\lambda_R = 495$ –590 nm. The polychromator dispersion was adjusted to cover a 1000 cm^{-1} probe range. The Stokes Raman signal was recorded by chopping the Raman beam, with actinic excitation at $\lambda_{ac} = 460$ nm. In this registration scheme, signals at negative pump–probe delays correspond to ground-state Raman contributions (from both solute and solvent). For positive delays, these contributions are eliminated by subtracting the signals at negative delays. 50–100 pump–probe scans were averaged to improve the signal-to-noise.

2.5. Computational Methods. Electronic structures and aspects of the potential energy surface for the $n\pi^*(S_1)$ and $\pi\pi^*(S_n)$ states (in our calculations, the latter was consistently identified as S_2 , and we use this designation instead of S_n when reporting computational results) were studied with XMCQDPT2 multistate multiconfiguration perturbation theory,⁵⁵ implemented in the Firefly 8.1 software,⁵⁶ which is partially based on GAMESS(US).⁵⁷ We used the cc-pVTZ basis set, and the core electrons were frozen on the PT2 stage. No symmetry constraints were applied. The CASSCF reference was constructed with the (14,12) active space covering the two lone pairs of the nitrogen atoms plus 5π and $5\pi^*$ orbitals, that is, those excluding the two energy-lowest nodeless and two highest trinodal phenyl orbitals. The XMCQDPT2 model space included the 12 lowest CASSCF roots. We found that the zero-order XMCQDPT2 density for the S_1 state is based almost entirely on the second CASSCF root, except for the trans–*cis* transition regions where the diminished S_1 – S_0 gap prompted the interaction of the two states. Therefore, we used either the pure-state CASSCF solutions or equal weight averaging over the two lowest roots. On the contrary, to correctly recover the trans– S_2 state, we had to use averaging over at least five CASSCF roots (fourth to eighth).

Nonresonant Raman spectra were calculated with the PRIRODA software,⁵⁸ which features a fast resolution-of-identity (RI) for the GGA functionals. We used the built-in TZ2P basis set ((11s6p2d)/[6s3p2d] for the first row atoms and (5s1p)/[3s1p] for hydrogens) and the PBE exchange–correlation functional.⁵⁹ The Hessian was computed analytically for the ground state and by numerical differentiation of the TDDFT analytic gradients for the excited state. To obtain the nonresonant Raman intensities, we combined the normal modes with the static polarizability derivatives computed for both states via numerical differentiation of the energy gradient over the electric field.

3. RESULTS AND DISCUSSION

3.1. Solvent Contribution to TA. Typical TA kinetics from *n*-hexane and from *trans*-azobenzene in *n*-hexane upon $n\pi^*$ (444 nm) excitation are shown in Figure 2. The curves have been corrected for the chirp of the probe supercontinuum. At early delays, $t < 0.2$ ps, signals are dominated by the solvent contribution (green lines). This is because the sample having absorbance $A \approx 1$ at 320 nm has $A \leq 0.02$ at 444 nm, and the solute signal there is weak accordingly. The solvent response was measured separately under identical conditions and then subtracted to result in the solute transient spectra. The latter are considered to be reliable from $t = 0.08$ ps onward. (See also Figure S2 in the Supporting Information.)

3.2. TA Spectra upon $n\pi^*(S_1)$ Excitation. Figure 3 shows TA spectra of *trans*- and *cis*-azobenzene in acetonitrile upon $n\pi^*$ (444 nm) excitation. Bleach and stimulated emission (SE) are negative, excited-state absorption (ESA) is positive, and the total signal is the sum of bleach, SE, and ESA.

For *trans*-azobenzene (at left), one distinguishes three ESA bands at 360, 390, and 520 nm and the bleach band at 320 nm. The SE band is peaked around 560 nm (see Figure 7) but not seen directly because it is overcompensated by stronger ESA. The ESA bands decay biexponentially with $\tau_1 = 0.3$ to 0.4 ps and $\tau_2 = 2.5$ to 3.5 ps (see kinetics in Figure 4), while the bleach first increases between 0.2 and 1 ps (top and middle frame) and then decays monoexponentially with 16 ps, as seen in Figure 3 bottom (and in Figures 4 and 5).

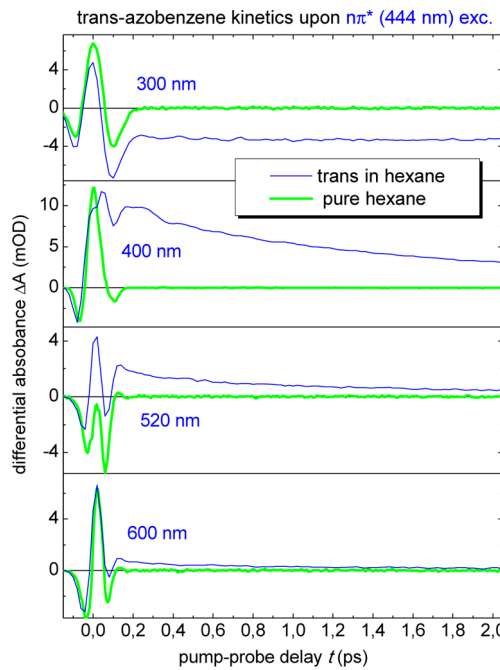


Figure 2. TA kinetics at various probe wavelengths from trans-azobenzene upon $n\pi^*$ (444 nm) excitation in hexane (blue lines). For $t < 0.2$ ps, the signal is dominated by the solvent contribution, measured independently (green). The solvent signal has been eliminated (subtracted) for all following TA spectra. More pump–probe kinetics are shown in the Supporting Information, Figure S2.

The cis evolution is shown at the right of Figure 3 for the same (as for trans) pump–probe delays. Early spectra (top) reveal ESA bands at 334 and 540 nm. They are similar to those of trans, but ESA3 is shifted more to the red, while ESA 1,2 are shifted to the blue and not resolved. The early evolution is fast (~ 0.1 ps) and strongly nonexponential. Ground-state products, which appear at $t = 0.3$ ps, are recognized by a rising absorption peak at 320 nm, which does not shift with time. (See also Figure S3 in the Supporting Information.) After 0.3 ps, the signal about 320 nm grows exponentially with $\tau = 1.1$ ps (Figure 3, middle, and kinetics in Figures 4 and 5). Traces of vibrational cooling are recognized at $t > 4$ ps (Figure 3, bottom right) as weak decay in the red wing of the absorption band and as a corresponding rise at the peak.

Transient spectra of the $\pi\pi^*$ bleach region are presented here for the first time. Evolution in this range has not been previously reported because the probe continuum is usually generated with the 800 nm fundamental, which prevents probing below 340 nm. In the present setup the continuum is generated at 400 nm, extending the range to 270 nm. The lower panels of Figure 3 allow a crucial comparison of trans and cis spectra at long delays. The current view^{23–32} attributes the change in late trans spectra to vibrational cooling. However, this interpretation is inconsistent with the cis evolution, which shows directly that the cooling contribution is negligible. Therefore, the trans spectra after 4 ps should reflect population decay, namely, the $S_1 \rightarrow S_0$ relaxation.

3.3. Normalization of TA Spectra to the Same Population. Consider late trans-azobenzene spectra (at $t = 100$ ps, Figure 3) when the isomerization is complete and products are mixtures of ground-state trans and cis isomers. Let n_0 and n , ($n_0 - n$) be the initially excited population and that of

cis and trans products, respectively. Then, the late spectrum is given by

$$\Delta A(\lambda, \infty) = n \cdot [A_c(\lambda) - A_t(\lambda)] = Y^{tc} n_0 [A_c(\lambda) - A_t(\lambda)] \quad (2)$$

where $A_c(\lambda)$ and $A_t(\lambda)$ are cis and trans absorption spectra and $Y^{tc} = n/n_0$ is the trans-to-cis isomerization yield. For the cis-to-trans reaction, eq 2 also holds by interchanging “t” and “c” indices. Thus, the late spectra can be fitted with the difference spectrum $[A_c(\lambda) - A_t(\lambda)]$, as illustrated in Figure S3 in the SI. The fits are good, confirming the assumption that the product mixture consists of cis and trans species only. Taking the yields from the literature,^{18,19} eq 2 allows us to normalize transient spectra to a given population, for a precise comparison of trans and cis evolutions under $n\pi^*$ or $\pi\pi^*$ excitation. Next, we restore the initial bleach

$$\Delta A_B(\lambda, 0) = -n_0 A_t(\lambda) = \frac{\Delta A(\lambda, \infty)}{Y^{tc}} \frac{1}{[1 - A_c(\lambda)/A_t(\lambda)]} \quad (3)$$

from the late signal $\Delta A(\lambda, \infty)$. Because the bleach is often overlapped with ESA of a priori unknown strength, the initial bleach signal cannot be taken directly from the early spectra, but it can be calculated by eq 3, provided the yield Y^{tc} is known. By modeling the bleach and product evolution, one can then separate the ESA evolution. We apply this approach in the next subsection.

3.4. TA Kinetics upon $n\pi^*$ Excitation.

Population kinetics are analyzed with band integrals⁴⁰

$$I(\lambda_1, \lambda_2, t) = \int_{\lambda_1}^{\lambda_2} \Delta A(\lambda, t) d\lambda/\lambda \quad (4)$$

where (λ_1, λ_2) is the integration region, which is chosen to eliminate the effect of spectral shifts. Figure 4 shows the early evolution of ESA and bleach. For trans-azobenzene (at left), the ESA signal decays biexponentially with $\tau_1 = 0.33$ to 0.45 ps and $\tau_2 = 2.4$ to 3.3 ps, with the spread in the decay times indicating nonexponential behavior. The latter is more pronounced for cis-azobenzene (at right), where exponential fits ($\tau = 1.1$ ps) apply only after $t = 0.3$ ps, whereas the earlier evolution is strongly nonexponential.

Consider the bleach evolution of trans in more detail (Figure 4, top left). The bleach (i.e., negative induced absorption) first increases with $\tau_1 = 0.35$ ps and after 1 ps decays with 17 ps. The initial decrease in absorbance will be interpreted as ESA decay because the true bleach (that is, deficiency of S_0 population) cannot increase after excitation; it may only decrease with time. Thus, the short evolution with $\tau_1 = 0.3$ ps and $\tau_2 = 3$ ps should reflect processes in S_1 , while the bleach itself is constant on this time scale.

Long-time bleach evolutions following $n\pi^*$ excitation are compared in Figure 5. For trans, the recovery is mono-exponential with $\tau_B = 16.1$ ps. On the basis of the previous discussion, we attribute the corresponding process to $S_1 \rightarrow S_0$ relaxation and not to ground-state vibrational cooling. With this assignment and with the initial bleach from eq 3, one can model the transient bleach and product spectra and subtract them from the measured ones to isolate the pure ESA contribution. The result is presented in Figure 6. It is seen that a new ESA4 band rises on a 1 ps scale at 300 nm, while the original ESA 1,2,3 bands disappear on the same time scale. Apparently, ESA4 corresponds to an intermediate S_{1t}^D (where superscript D

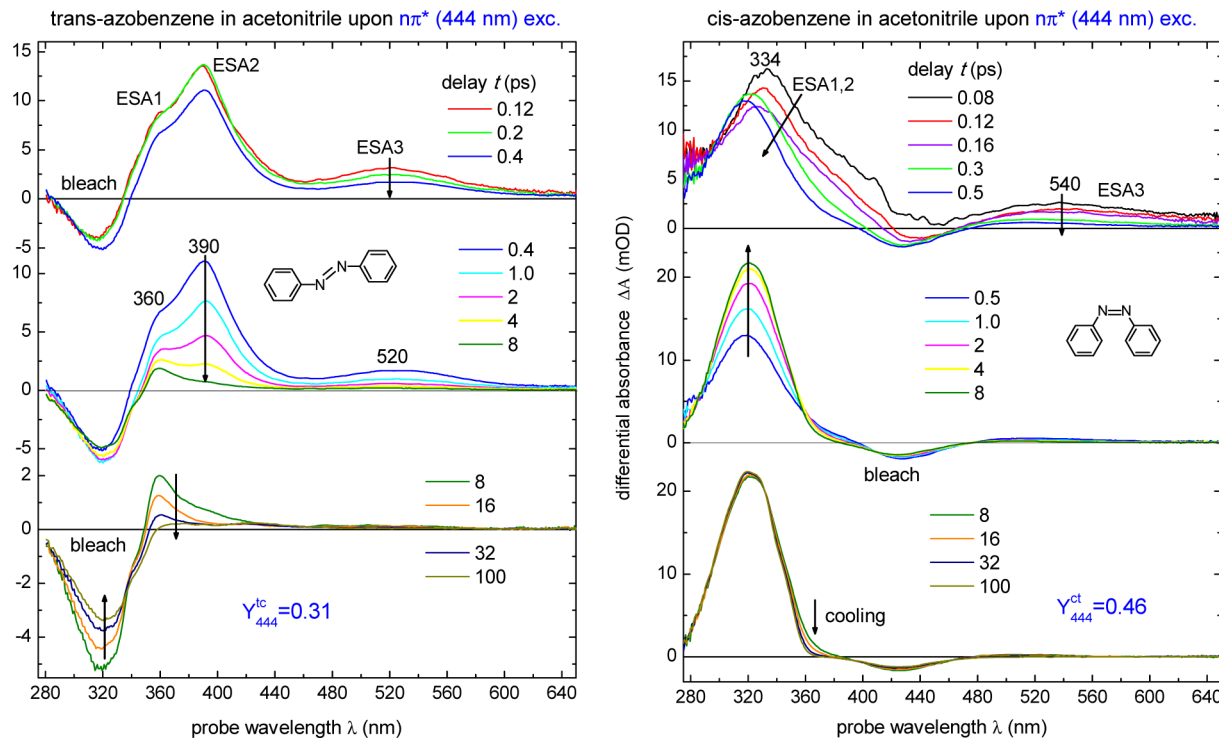


Figure 3. TA spectra of *trans*- and *cis*-azobenzene in acetonitrile upon $n\pi^*(S_1)$ excitation. Bleach is negative and excited-state absorption (ESA) positive; arrows indicate the evolution. For $t < 0.2$ ps, the corresponding solvent signal has been subtracted. For *trans* (at left), one observes bleaching at 320 nm and ESA bands at 360, 390, and 520 nm. ESA decay biexponentially with $\tau_1 = 0.3$ to 0.4 ps and $\tau_2 = 2.5$ to 3.5 ps (see Figure 4), while the bleach first increases (before 1 ps) and then recovers with 16 ps. At $t = 100$ ps, the evolution is complete, the product is a mixture of *trans* and *cis* species, and the bleach signal is proportional to $[A_c(\lambda) - A_t(\lambda)]$. For *cis*-azobenzene (at right), ESA bands at 334 and 540 nm are similar to those of *trans*, but ESA3 is red-shifted, while ESA2 is blue-shifted, and ESA1 is no longer resolved. Early decay with ~ 0.1 ps is strongly nonexponential. Ground-state *cis* and *trans* products are seen after $t = 0.3$ ps. Further evolution (growth at 320 nm) is exponential with 1.1 ps. The effect of vibrational cooling is negligible, as seen in the spectra after 4 ps. Spectra at 100 ps are proportional to $[A_t(\lambda) - A_c(\lambda)]$. (See fits in Figure S3 in the Supporting Information.) Isomerization yields Y from refs 18 and 19 are indicated.

denotes “dark” in emission), which decays with 16 ps to the ground state via an S_1/S_0 conical intersection.

3.5. Transient Fluorescence of *trans*-Azobenzene upon $n\pi^*$ Excitation. Time-resolved fluorescence spectra and kinetics $I(\nu, t)$ of *trans*-azobenzene in *n*-hexane are displayed in Figure 7. The magic-angle signal $I = I_\perp/(1 - 0.4 \exp(-t/\tau_R))$ was constructed from I_\perp with $\tau_R = 17$ ps for the rotational diffusion time in *n*-hexane (Table 2). The transient spectra reveal a dynamic Stokes shift and decay on multiple time scales. The spectral shift is biexponential, $t_1^{\text{shift}} = 0.26$ ps (70%), $t_2^{\text{shift}} = 30$ ps (30%); the intensity decay is best described by four exponential terms with $t_1 = 0.3$ ps (48%), $t_2 = 2.6$ ps (18%), $t_3 = 12.2$ ps (19%), and $t_4 = 66.0$ ps (13%). Note that the first three components closely reproduce our TA results (Figures 4 and 5, Table 1). The fourth (66 ps) is more difficult to explain. Its small amplitude of 1/3 photon/s may be due to impurities.

Broadband transient fluorescence spectra from *trans*-azobenzene are shown here for the first time. The fast fluorescence decays t_1 and t_2 agree with previous reports.^{30,31} The 12 ps component has not been previously reported. It agrees with our TA results and further supports the existence of the long-lived intermediate S_{1t}^D .

The fast fluorescence decay, with $t_1 = 0.3$ ps, nearly equals the fast spectral shift $t_1^{\text{shift}} = 0.26$ ps. The correlation suggests the following interpretation. The time t_1 should correspond to escape of the excited population from the FC region, resulting in the concomitant fluorescence shift and decay, with the decay

being due to a drop in the oscillator strength. The longer $t_2 = 2.6$ ps decay would reflect further population transfer along the S_1 surface, from the S_{1t}^L minimum (still close to the FC point) to the S_{1t}^D intermediate. The transfer time t_2 is relatively long and suggests a barrier that can be estimated as

$$E = k_B T \ln(t_2/t_0) \quad (5)$$

Taking $t_0 = 0.1$ ps for the barrierless transfer (as in *cis*-azobenzene), one gets $E = 8$ kJ/mol. The barrier agrees with the existence of a stationary S_1 point from our calculations. Note that the assignment of the fast decay to the escape from the FC region has been previously proposed;^{23–25} our results support that interpretation.

3.6. TA Spectra and Kinetics upon $\pi\pi^*(S_n)$ Excitation.

Figure 8 shows TA spectra of *trans*- and *cis*-azobenzene in acetonitrile upon $\pi\pi^*$ (310 nm) excitation. Early delays, $t = 0.08$ to 0.2 ps, reveal ultrafast decay in the red and growth in the blue, with an isosbestic point at $\lambda = 440$ nm for *trans* and at $\lambda = 420$ nm for *cis*. This ultrafast evolution on a 0.1 ps scale is reasonably associated with the $S_n \rightarrow S_1$ relaxation.²⁸ Note, however, that the subsequent S_1 evolution (Figure 8) is different from that upon the direct $n\pi^*(S_1)$ excitation. For *trans*, the major difference is that ESA1 and ESA2 (at 360 and 390 nm) are not resolved any longer. For *cis*, the differences are more dramatic. For example, at $t = 0.3$ ps, one clearly observes ESA peaks at 360 and 390 nm, which are characteristic for the *trans* isomer, indicating that a substantial fraction of *cis* population isomerizes to *trans* via an S_n/S_1 conical intersection.

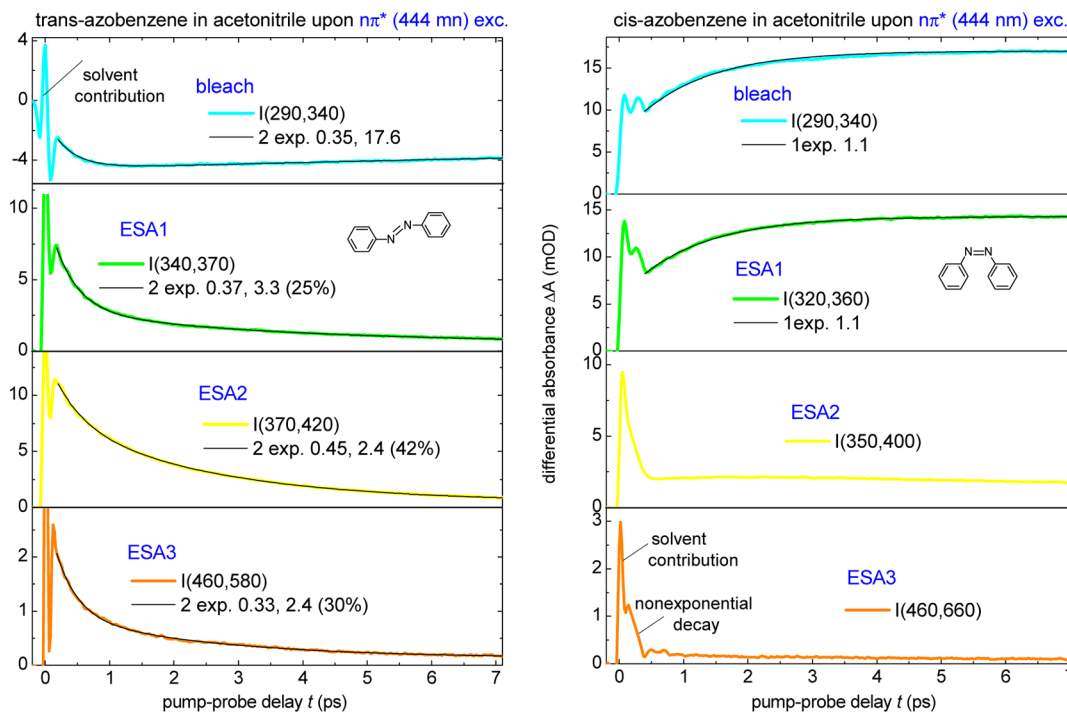


Figure 4. Short-time trans and cis evolution in acetonitrile upon $n\pi^*(S_1)$ excitation from integral kinetics $I(t) = \int \Delta A(\lambda, t) d\lambda / \lambda$. Exponential fit parameters τ_1, τ_2 (in ps) are indicated. For *trans*-azobenzene, $\tau_1 = 0.33$ to 0.45 ps and $\tau_2 = 2.4$ to 3.3 ps. The spread of decay constants indicates nonexponential evolution. The latter is more pronounced in *cis*-azobenzene, where exponential fits are inapplicable at early time (but one can still attribute a time scale of 0.1 ps to the early evolution). Signals about time zero are dominated by the solvent response.

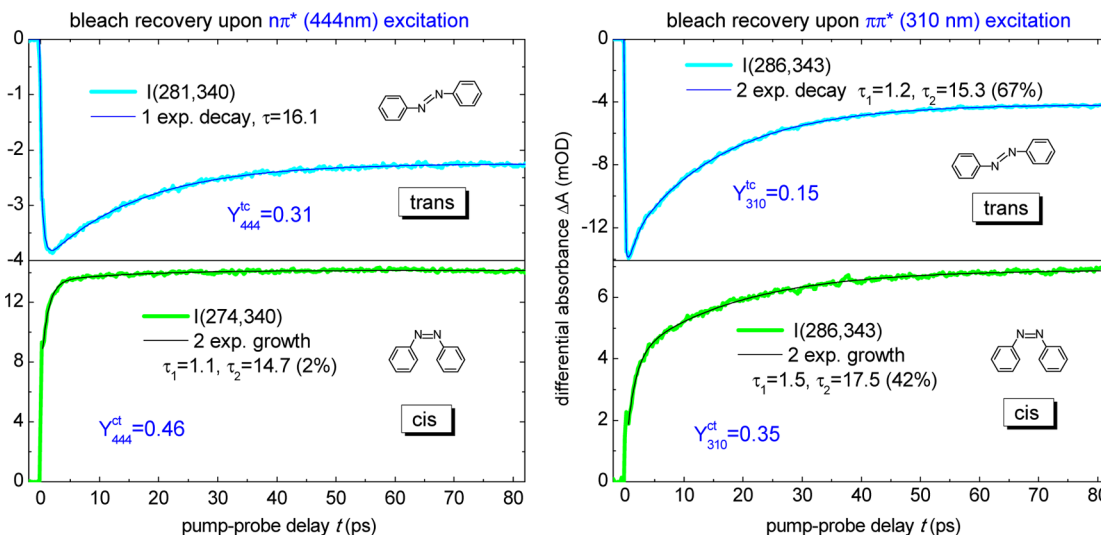


Figure 5. Long-time bleach evolution in acetonitrile from kinetics $I(\lambda_1, \lambda_2) = \int \Delta A(\lambda, t) d\lambda / \lambda$. For *trans*-azobenzene upon $n\pi^*(S_1)$ excitation (top left), the bleach initially increases on a 1 ps scale and then recovers with $\tau = 16.1$ ps. The latter process corresponds to $S_{1t}^D \rightarrow S_0$ relaxation. With $\pi\pi^*(S_n)$ excitation of *trans* (top right), one observes a fast ($\tau_1 = 1.2$ ps) additional decay, reflecting a new relaxation channel. A slow ($\tau_2 = 15.3$ ps) decay is close to that following $n\pi^*$ excitation. For *cis*-azobenzene upon $n\pi^*$ excitation (bottom left), the bleach recovers with $\tau_1 \approx 0.1$ ps (~50%) and $\tau_2 = 1.1$ ps, different from the evolution of *trans*, implying other isomerization paths with no common intermediate. With $\pi\pi^*$ excitation of *cis* (bottom right) the 17.5 ps component is similar to that for the *trans* isomer, suggesting isomerization to *trans* via an S_n/S_1 conical intersection and further relaxation to S_0 . Isomerization yields Y from refs 18 and 19 are indicated.

Short-time kinetics of *trans*-azobenzene upon $\pi\pi^*$ excitation are shown in Figure 9. An ultrafast 0.1 ps decay reflects the previously mentioned $S_n \rightarrow S_1$ relaxation. The kinetics are generally different from those under $n\pi^*$ excitation. In particular, the bleach band (on top) reveals an additional 1.2 ps component. Long-time bleach kinetics are presented in Figure 5 at right. For *trans*-azobenzene, the bleach recovery is

biexponential, with $\tau_1 = 1.2$ ps and $\tau_2 = 15.3$ ps. The slow component τ_2 is very similar to that observed with the $n\pi^*$ excitation and hence should correspond to the $S_{1t}^D \rightarrow S_0$ isomerization path, whereas the short $\tau_1 = 1.2$ ps decay reflects an additional $S_n \rightarrow S_0$ relaxation channel. For *cis*-azobenzene upon $\pi\pi^*$ excitation, a 17.5 ps decay is close to that observed

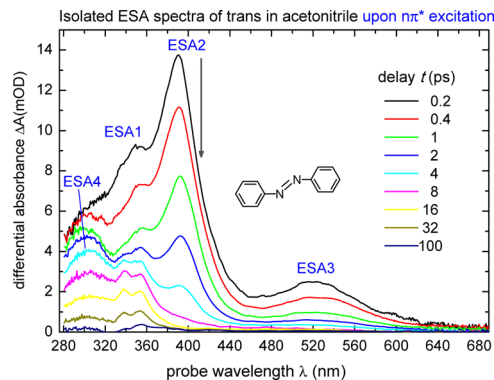


Figure 6. ESA spectra of trans-azobenzene in acetonitrile upon $n\pi^*(S_1)$ excitation, derived from Figure 3 by subtracting bleach and product spectra (neglecting SE). An ESA4 band at 300 nm develops on a 1 ps scale, while ESA 1,2,3 decays. The ESA4 band is associated with the S_{1f}^D intermediate, which relaxes to the ground state with 16 ps.

with the trans isomer, confirming the presence of S_1 trans population created via S_n/S_1 intersection.

Next, we quantitatively compare the cis and trans evolutions under different excitation. With eq 2, transient spectra can be normalized to the same excited population, as shown in Figure 10 for *trans*-azobenzene. Here isomerization yields at $t = 100$ ps fix the bleach ratio, $Y_{444}^c/Y_{310}^c = 2.1$,^{18,19} and accordingly determine the spectra at earlier delays. As seen at $t = 0.4$ and 1 ps, the ESA2 and ESA3 bands upon $\pi\pi^*$ excitation are weaker by a factor two compared with $n\pi^*$ excitation. It follows that 50% of excited trans species do not reach S_1 or reach a different S_1 region not accessible with $n\pi^*$ excitation. In connection to this, the previously mentioned fast (1.2 ps) bleach recovery may reflect a relaxation cascade $S_n \rightarrow S_1 \rightarrow S_0$ via that region.

A different picture of *trans*-azobenzene excited-state evolution upon $\pi\pi^*$ excitation has been proposed by Tahara and coworkers.^{27,28} They argued that the *entire* S_n population relaxes to the same S_{1f}^L region from which the $n\pi^*$ fluorescence occurs.²⁸ Their result was critically dependent on many

experimental parameters such as fluorescence yields or lifetimes of the $\pi\pi^*$ and $n\pi^*$ transitions. In particular, the lifetimes were reported to be 0.11 and 0.5 ps, respectively.²⁸ However, other reports^{25,30,31} and our Table 1 indicate different numbers deviating at least by 30%, that would affect the estimate of ref 28. We believe that our normalization procedure, given by eq 2, provides a more accurate comparison of the $\pi\pi^*$ and $n\pi^*$ evolution.

cis-Azobenzene transient spectra (after normalization to equal excited populations) are compared for $\pi\pi^*$ and $n\pi^*$ excitation in Figure 11. The spectra upon $\pi\pi^*$ excitation at $t \geq 0.2$ ps reveal the trans ESA bands at 360, 390, and 520 nm. The amplitudes of these bands, estimated with the help of Figure S4c in the Supporting Information (where $\pi\pi^*$ cis and $n\pi^*$ trans spectra are compared), allow us to conclude that ~30% of cis species isomerize to trans via S_n/S_1 conical intersection. Similarly Figure S4a in the Supporting Information compares the cis and trans ESA bands under $n\pi^*$ excitation. It follows that cis ESA is nearly five times weaker than that of trans. Interestingly, a similar intensity ratio of cis and trans ESA was also found for stilbene.⁴⁶

3.7. Solvent Viscosity, Polarity, and Proticity Effects.

Short-time kinetics of *trans*-azobenzene are practically independent of solvent viscosity and polarity, as seen from Figure 12 for $n\pi^*$ excitation and from Figure S6 in the Supporting Information for $\pi\pi^*$ excitation. Small differences in the bleach kinetics in acetonitrile are actually due to the long-time behavior. The long-time bleach evolution is sensitive to solvent polarity/proticity but not to the viscosity. This is clear from Figure 13, where bleach kinetics are compared for different solvents. Note that no dependence on viscosity can be discerned in hydrocarbons (*n*-hexane, *n*-decane, *n*-hexadecane), whereas in dichloromethane or perfluoro-*n*-hexane, the decays are slower and the isomerization yields are higher. Furthermore, in protic methanol, the recovery (isomerization) is faster than in *n*-hexane, and it is even faster in more protic ethylene glycol despite its very high viscosity.

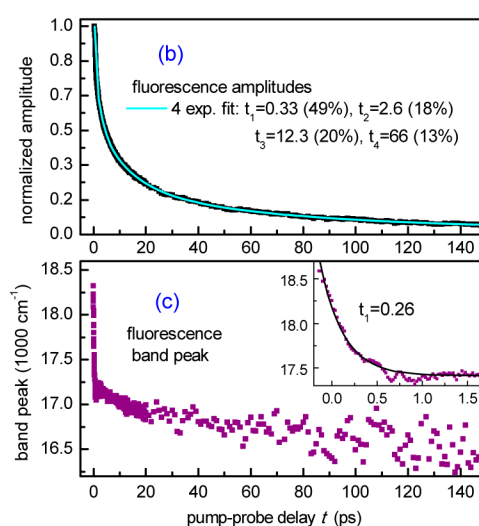
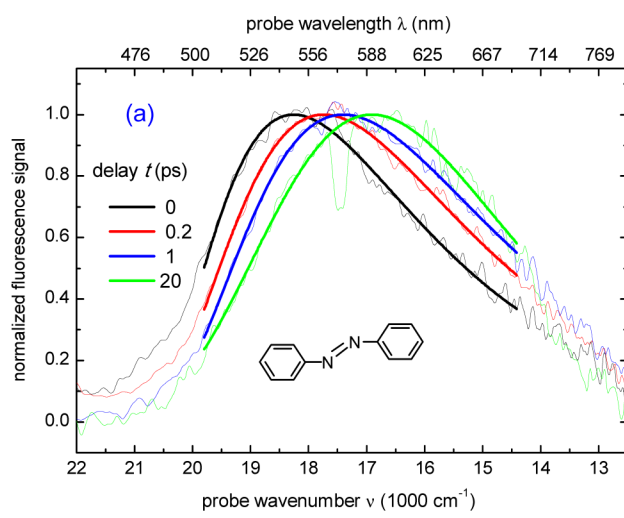


Figure 7. Transient fluorescence results for *trans*-azobenzene in *n*-hexane upon $n\pi^*$ (400 nm) excitation. Magic-angle spectra $I(\nu,t)$ were fitted with log normals. The peak intensity was 10 to 11 counts per 3 s. (a) Normalized spectra reveal a dynamic Stokes shift. (b) The signal decay is 4-exponential with $t_1 = 0.3$ ps (48%), $t_2 = 2.6$ ps (18%), $t_3 = 12.2$ ps (19%), and $t_4 = 66.0$ ps (13%). The first three times correspond closely to those from TA measurements. The t_4 component is small (1 photon per 3 s) and may come from impurities. (c) The Stokes shift reveals a fast $t_1^{\text{shift}} = 0.26$ ps and slow $t_2^{\text{shift}} = 30$ ps component. Note the coincidence $t_1^{\text{shift}} \approx t_1$.

Table 1. Band Peaks, Oscillator Strengths, and Decay Times of *trans*- and *cis*-Azobenzene in Acetonitrile

	band peak (nm)	oscillator strength ^c	nπ* exc.	decay in acetonitrile ^{a,b} ππ* exc.
trans-azobenzene				
nπ* band	320	0.35	16.1	1.2, 17 (67%)
nπ* band	444	0.006		
ESA1	356	0.2	0.37, 3.3 (25%)	0.24, 3.5 (38%)
ESA2	389	0.3	0.45, 2.4 (42%)	0.37, 2.3 (27%)
ESA3	519	0.1	0.33, 2.4 (30%)	1.0
ESA4	300	0.2	16.1	
<i>cis</i> -azobenzene				
ππ* band	280	0.10	1.1	1.5, 18 (42%)
nπ* band	439	0.02		
ESA1,2	334	0.1	0.1	
ESA3	540	0.02	0.1	

^aDecay times (in ps) and their amplitude (in %) from mono-, bi-, or tri-exponential fits. ^bUltrafast $S_n \rightarrow S_1$ decay, $\tau = 0.09$ ps, upon ππ* excitation is not shown here. ^cAbsorption oscillator strength: $f_A = (4.39 \times 10^{-9}/n) f\varepsilon(\nu) d\nu \approx 3 \times 10^{-9} \varepsilon \Delta\lambda/\lambda^2$.

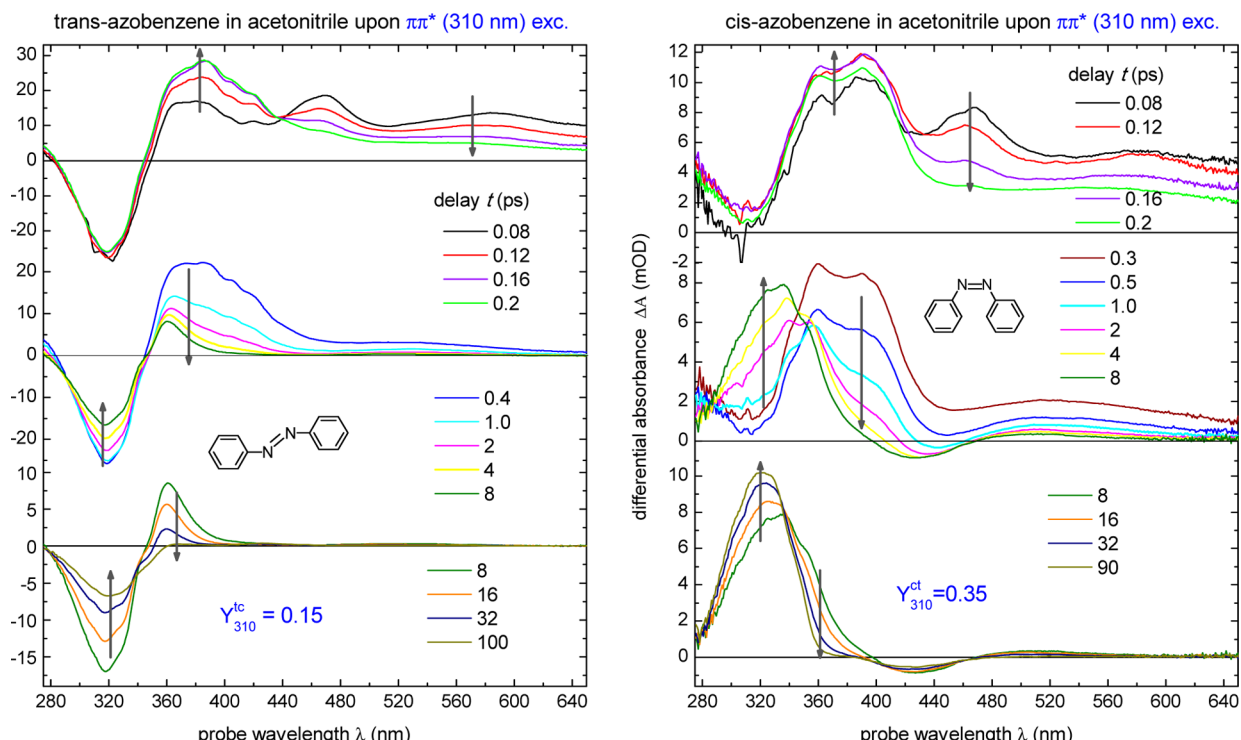


Figure 8. TA spectra of *trans*- and *cis*-azobenzene in acetonitrile upon ππ*(S_1) excitation. An early evolution ($t = 0.08$ to 0.2 ps, top) reflects $S_n \rightarrow S_1$ conversion with 0.09 ps. The further S_1 evolution deviates from that upon nπ*(S_1) excitation. For *trans* (at left), ESA1 and ESA2 are not resolved anymore. In the *cis* case (at right), a part of the relaxed S_1 population (25–30%) appears in the *trans* form, as evidenced by ESA bands at 360 and 390 nm. The latter are similar to those observed with nπ* excitation.

Once the early bleach signals are normalized to the same amplitude, their ratios at late time determine the corresponding isomerization yields. By using the yield in acetonitrile, other yields are calculated and given in Table 2. For example, in *n*-hexane, the isomerization yield is 1.3 times lower than in acetonitrile with both nπ* and ππ* excitation, in good agreement with the literature.^{18,19}

Anisotropy decays $\rho(\lambda, t)$ for *trans*-azobenzene in the bleach and ESA 1,2 regions are presented in Figure 14. The increase of in rotational diffusion time τ_R with viscosity agrees with the expected molecular reorientation behavior. Note that the ESA anisotropy decays faster (by 1.5 to 2 times) than the bleach anisotropy; the reason for this effect is unclear.

Figure 15 compares the dependence of bleach recovery τ_B (isomerization time) on the rotational diffusion time τ_R for *trans*-azobenzene (closed squares) and for *trans*-stilbene (open circles). The strong viscosity dependence for stilbene agrees with the torsional isomerization path. On the contrary, *trans*-azobenzene shows no viscosity dependence, suggesting a different isomerization mechanism.

3.8. Tables of Spectroscopic and Kinetic Data. Our TA and fluorescence results are summarized in Tables 1 and 2. Table 1 contains ESA peaks and oscillator strengths and decay times in acetonitrile upon nπ* and ππ* excitation. The ESA oscillator strengths are estimated from comparison with the bleach bands. The decay times are obtained from mono-, bi-, or

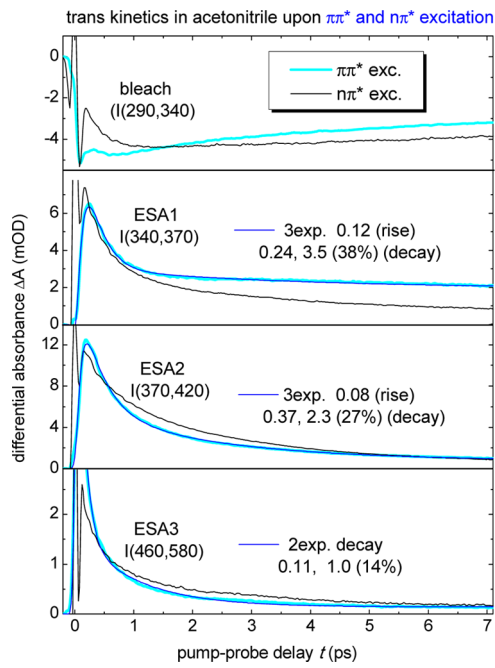


Figure 9. Short-time kinetics of *trans*-azobenzene in acetonitrile upon $\pi\pi^*(S_n)$ excitation (cyan) and upon $n\pi^*(S_1)$ excitation (black). An ultrafast ($\tau \approx 0.1$ ps) decay reflects $S_n \rightarrow S_1$ relaxation. The $\pi\pi^*$ and $n\pi^*$ evolutions are different.

tri-exponential fits. Table 2 collects rotational diffusion times τ_R (from bleach anisotropy decays), bleach recovery (isomerization) times τ_B , and isomerization yields Y in various solvents. The yields are estimated relative to the yield in acetonitrile.^{18,19} The bleach recoveries are monoexponential with $n\pi^*$ excitation and biexponential with $\pi\pi^*$ excitation. Reorientation times τ_R are derived from monoexponential fits presented in Figures S7 and S8 in the Supporting Information. Interestingly, the trans τ_R are slower than the cis τ_R . Furthermore, τ_R is slower with $\pi\pi^*$ compared with $n\pi^*$ excitation. These effects may be partially related to the difference in molecular size (hence different τ_R) of the cis and trans isomer and hence with the different isomerization yield upon $\pi\pi^*$ and $n\pi^*$ excitation.

Diua and coworkers³¹ reported for *trans*-azobenzene that the anisotropy decays on a subpicosecond scale in *n*-hexane, whereas such behavior was not observed in ethylene glycol. However, our observations (Tables 1 and 2) do not reproduce their results. We have shown that the isomerization kinetics (both short and long) are independent of the solvent viscosity, implying an identical isomerization mechanism in different solvents.

3.9. Femtosecond Stimulated Raman Spectra. Figure 16 presents our femtosecond stimulated Raman (FSR) results for *trans*-azobenzene. Ground-state S_0 Raman spectra are shown in the bottom panel, where the signal in the low-frequency range has also been magnified. In the middle are shown S_1 spectra recorded without (orange) and with (red) $n\pi^*$ actinic excitation, as detailed in a separate publication.⁵⁴ Here

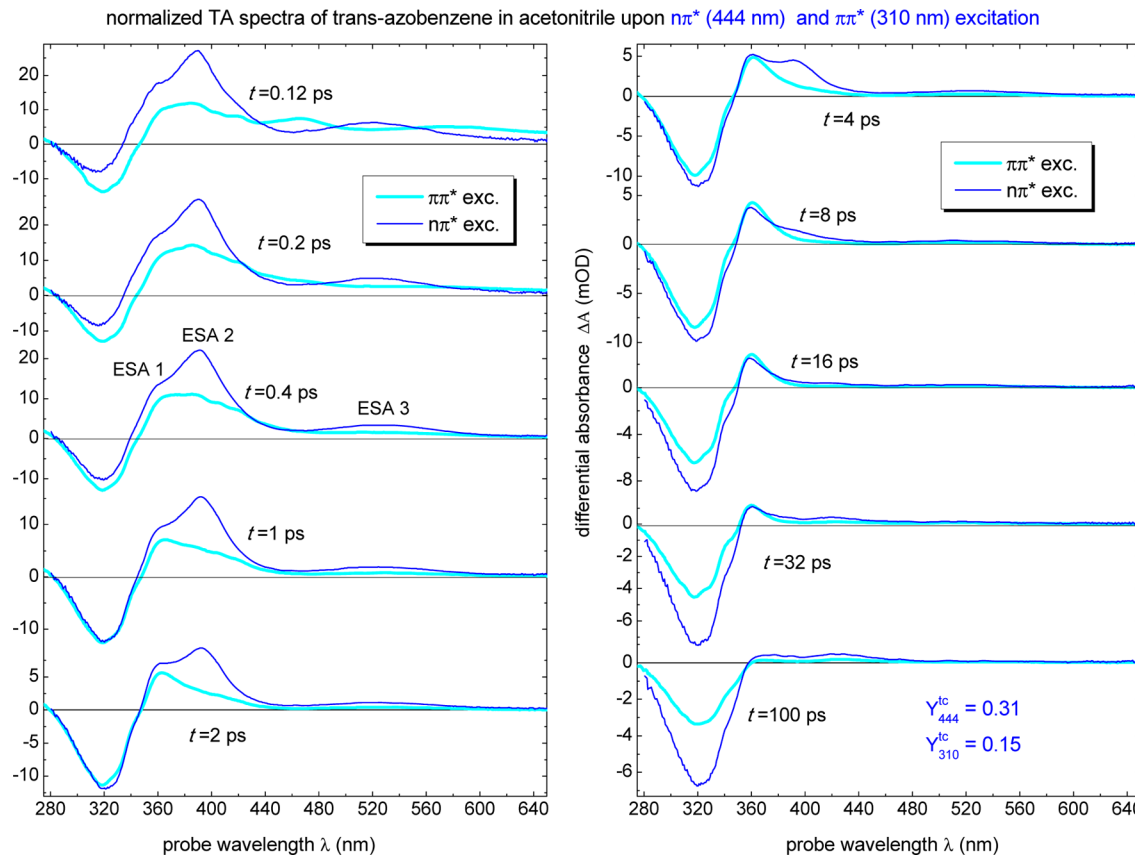


Figure 10. TA spectra of *trans*-azobenzene in acetonitrile with $n\pi^*(S_1)$ or $\pi\pi^*(S_n)$ excitation, normalized to equal populations excited initially. Isomerization yields^{18,19} $Y_{444}^{tc} = 0.31$ and $Y_{310}^{tc} = 0.15$ fix the ratio of late spectra at $t = 100$ ps and thus determine the spectra at earlier delays. Upon $\pi\pi^*$ excitation ESA2 and ESA3 bands are suppressed, indicating that up to 50% of population relaxes to an S_1 region, which is not accessible with $n\pi^*$ excitation.

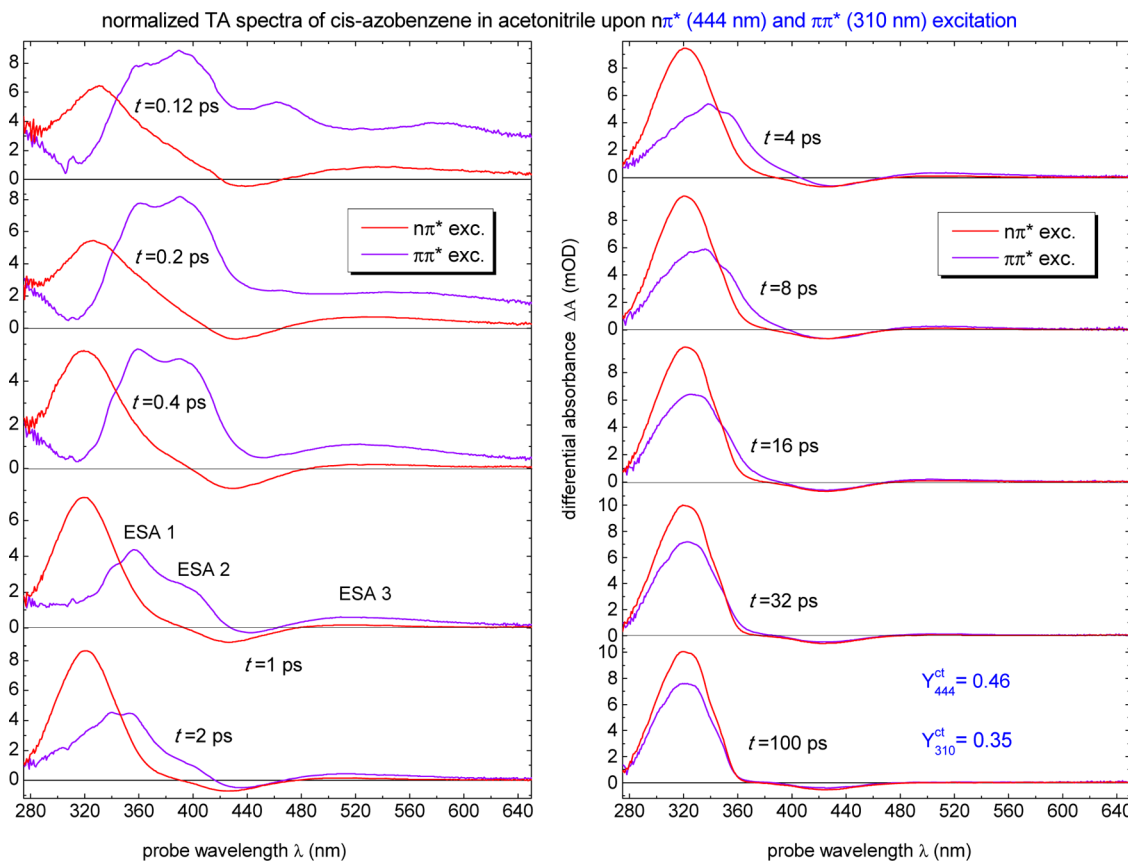


Figure 11. TA spectra of *cis*-azobenzene in acetonitrile with $n\pi^*(S_1)$ or $\pi\pi^*(S_n)$ excitation, normalized to *equal* population excited initially. Under $\pi\pi^*$ excitation, one observes (at $t > 0.2$ ps) trans ESA 1,2,3 bands that correspond to the *cis*-to-trans isomerization yield of 0.3 via S_n/S_1 conical intersection.

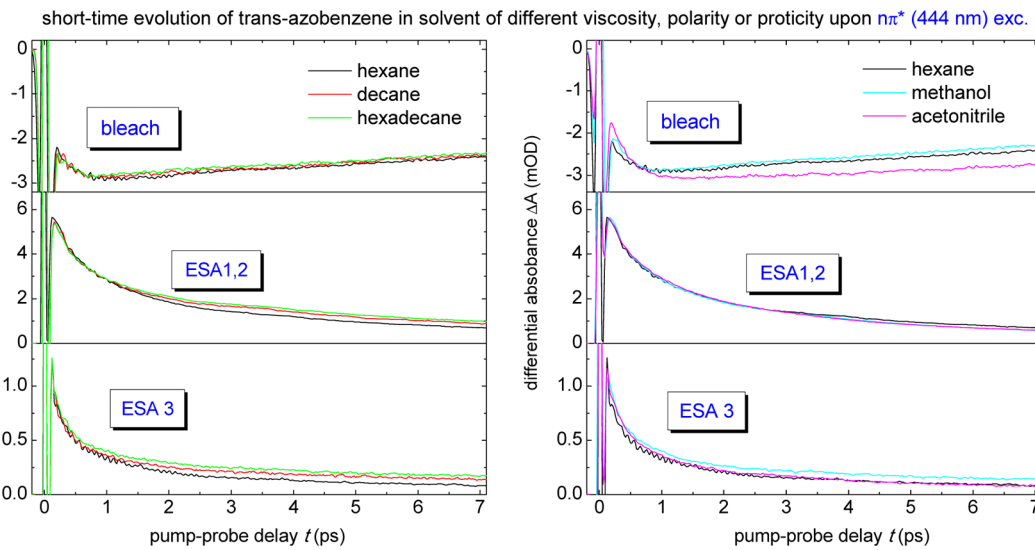


Figure 12. Short-time kinetics of trans-azobenzene upon $n\pi^*$ excitation in solvents of various viscosity, polarity, and proticity.

the real intensity of the orange spectrum is reduced 10 times, illustrating the power of ground-state measurements. The top frame shows S_n Raman spectra upon $\pi\pi^*(S_n)$ excitation. The S_n spectra are short-lived and decay with $\tau = 0.09$ ps due to $S_n \rightarrow S_1$ internal conversion. (See kinetics in Figure S12 in the SI.) The decay constant agrees with the TA results (Figures 8 and 9) and with the literature.²⁸

Figure 17 shows S_0 Raman spectra of *cis*-azobenzene. Unfortunately, excited S_1 spectra are extremely weak and therefore, not shown here (although an example is given in Figure S14 in the SI). The trans S_n spectra and cis S_0 spectra are published here for the first time. The trans S_1 spectra differ from a previous report,²⁷ as discussed by us in ref 54.

3.10. Calculation of Potential Energy Surface. In *trans*-azobenzene, our XMCQDPT2 data predict planar and C_{2h}

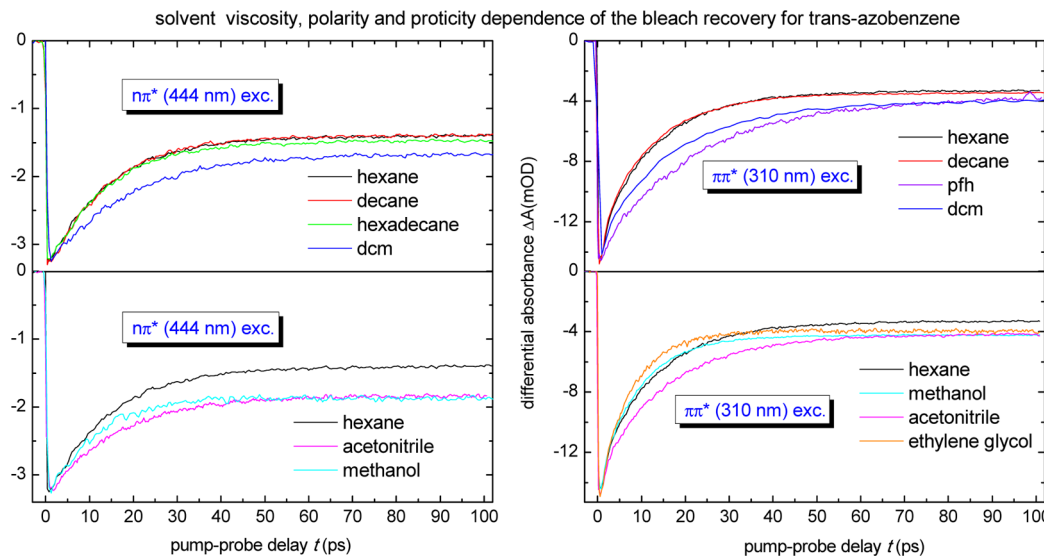


Figure 13. Long-time bleach kinetics of *trans*-azobenzene in various solvents. The decay depends on viscosity (top) and polarity (bottom right) but more strongly depends on proticity. It is faster for methanol and even faster for ethylene glycol despite its high viscosity. For dichloromethane (dcm), the $\pi\pi^*$ excitation was at 326 nm. pfh: perfluoro-*n*-hexane.

Table 2. Rotational Diffusion Time, τ_R , Bleach Recovery Time, τ_B , and Isomerization Yields, Y , of *trans*- and *cis*-Azobenzene in Various Solvents

solvent	viscosity ^c (20 °C)	rotational diffusion time τ_R^a		bleach recovery τ_B^a		isomerization yield Y^b	
		$n\pi^*$ exc.	$\pi\pi^*$ exc.	$n\pi^*$ exc.	$\pi\pi^*$ exc.	$n\pi^*$ exc.	$\pi\pi^*$ exc.
<i>trans</i> -azobenzene							
hexane	0.31	17	20	13.6	1.0, 14 (65%)	0.24	0.12
decane	0.93	43	53	13.6	1.9, 13 (60%)	0.24	0.13
hexadecane	2.54	100		13.5		0.25	
perfluorohexane	0.66		45 ± 12		20		0.14
dichloromethane	0.44		28	18.7	2.4, 18 (75%)	0.29	0.14
acetonitrile	0.36	19	22	16.1	1.2, 17 (65%)	0.31 ^d	0.15 ^d
methanol	0.59	29	36	10.9	1.1, 9.2 (75%)	0.32	0.15
ethylene glycol	22				1.0, 7.6 (76%)		0.14
<i>cis</i> -azobenzene							
hexane	0.31	10		1.4	1.4	0.55	0.31
acetonitrile	0.36	14	10	1.1	1.1	0.46 ^d	0.35 ^d
methanol	0.59	18		1.1	1.1	0.45	
Y^{ct}							

^aTime constants in picoseconds from monoexponential or biexponential fits (with ±10% accuracy). ^bIsomerization yields from this work are derived by comparison with those in acetonitrile.^{18,19} ^cIn centipoise (cp). ^dIsomerization yields from refs 18 and 19.

symmetric stationary points in both S_1 and S_2 states. This is in agreement with the previous CASSCF(14,12) calculations.³⁸ On the contrary, a more recent CASPT2 and TDDFT analysis suggests instability of the C_{2h} geometry along the torsional coordinate;⁴⁰ however, this study further predicts a completely barrierless rotational coordinate in S_1 , which is inconsistent with the available experimental results. Somewhere in between are the ROKS results that predict stationary point having a considerably twisted geometry, with a C—N=N—C dihedral angle of 115–130°^{12,39} and CASSCF with smaller active spaces.³⁴ Such rotated minima could be candidates for the dark stationary point in S_1 , whose presence we deduce from our experimental data. However, all calculations predict either the planar or else the rotated minimum but not both together. Furthermore, the ROKS minima are not reproduced by CASSCF(14,12) and CASPT2 recomputations.¹²

We are presently performing 1D relaxed scans of the PES of S_1 along the twisting coordinate and the inversion coordinate.³⁷ For the twisting coordinate, we observe that the molecule

retains C_2 symmetry in the range of twisting angles $C_1NN'C'_1$ from 180° (trans) to ca. 120° where the S_0 – S_1 gap reduces to 0.8 eV. Further twisting causes symmetry breaking associated with the interaction of the two states, and the molecule relaxes toward an asymmetric state, which is analogous to the perpendicular phantom state in stilbene.^{46,60} The barrier of 0.15 eV is located near 114°. The latter value is in agreement with the bleach recovery time of 16 to 17 ps, not with the much faster decay of the ESA bands. Also, the twisting pathway does not seem to involve an apparent dark intermediate in S_1 . Formally, this role could be played by the above asymmetric state (which, of note, seems to lie some 0.05 eV above the trans- S_1 stationary point), but presently we find the S_1/S_0 intersection to be too close and accessible to account for a 16 ps lifetime.

Scanning of the inversion coordinate starting from the planar trans- S_1 geometry reveals a much steeper energy elevation by at least 0.4 eV. This is inconsistent with the isomerization on the picosecond time scale and therefore rules out this type of

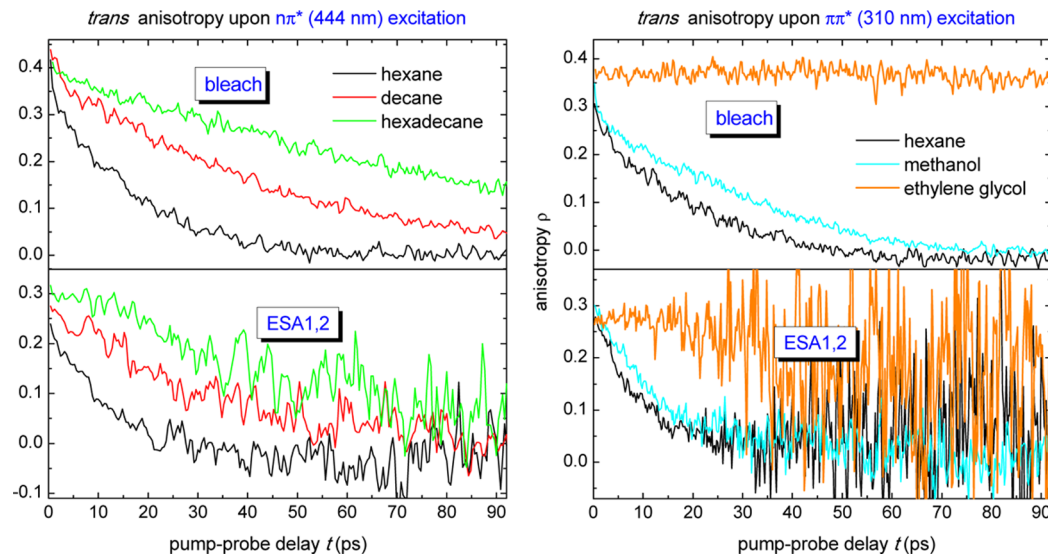


Figure 14. *trans*-Azobenzene anisotropy $\rho(\lambda,t) = (\Delta A_{\parallel} - \Delta A_{\perp})/(\Delta A_{\parallel} + 2\Delta A_{\perp})$ decays in the bleach (top) and ESA region upon $n\pi^*$ or $\pi\pi^*$ excitation. ESA anisotropies decay slightly faster than the bleach anisotropies.

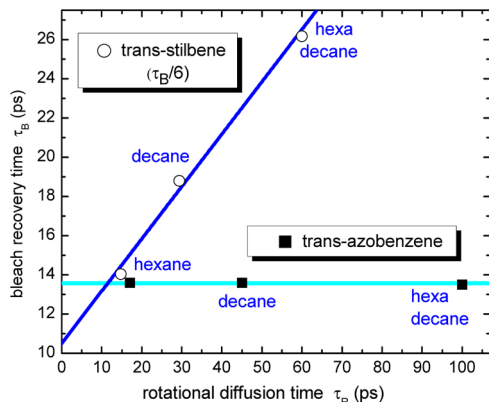


Figure 15. Bleach recovery (isomerization) time τ_B as a function of rotational diffusion time τ_R for *trans*-azobenzene (closed squares) and *trans*-stilbene (open circles, here τ_B is divided by 6). *trans*-Azobenzene shows no viscosity dependence, ruling out torsion and suggesting the hula-twist pathway. Interestingly, despite similar molecular size, τ_R for azobenzene is 1.5 times longer than that for stilbene, indicating extra friction due to interaction with the nitrogen unpaired electrons.

motion in its pure form. (Interestingly, the molecule tends to remain mostly planar along this inversion scan, even if an asymmetry was introduced in the starting coordinates.) Thus, our initial findings are rather in agreement with the previous theoretical works^{12,40} than with the present experimental observations of the viscosity independence of the process. Possibly the controversy may be resolved through consideration of a mixed pathway involving a certain degree of twisting combined with inversion or “hula-twist”-like motion.

3.11. Calculation of Raman Spectra. In *trans*-azobenzene, the S_0 and S_1 states were found to have proper C_{2h} symmetric stationary points both at the DFT (TDDFT) and at the XMCQDPT2 levels. On the contrary, the behavior of the $\pi\pi^*(S_2)$ state under TDDFT optimization proved elusive. We observed, somewhat counterintuitively, symmetry breaking via rotation of one of the phenyl rings, upon which the dominant HOMO-1 \rightarrow LUMO contribution becomes mixed with the other excitations. However, the symmetry-less XMCQDPT2 calculations do not confirm such symmetry breaking at present.

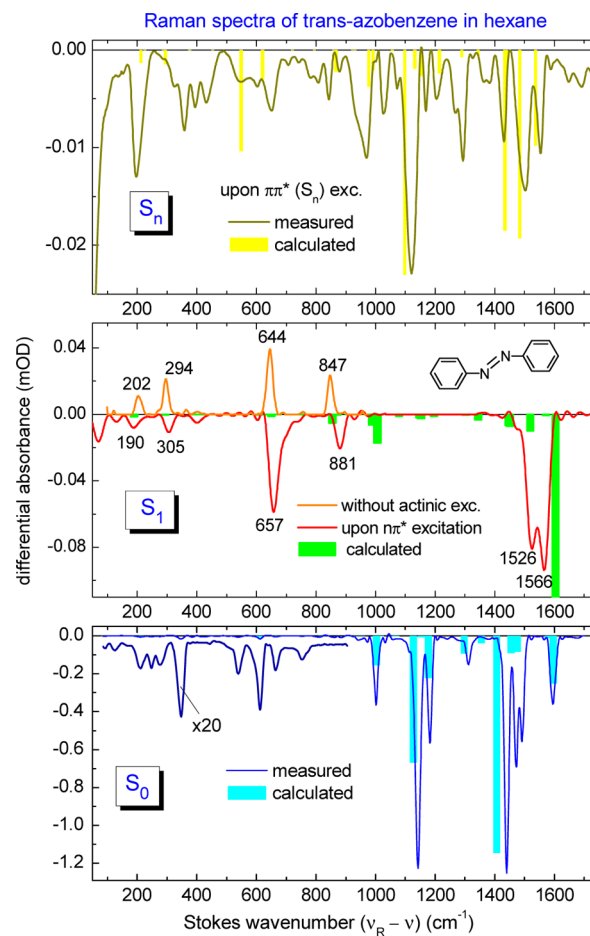


Figure 16. FSR spectra of *trans*-azobenzene in *n*-hexane: in S_0 with Raman pump at $\lambda_R = 540$ nm (bottom); in S_n upon $\pi\pi^*(310$ nm) actinic excitation, with $\lambda_R = 580$ nm (top); in S_1 upon $n\pi^*(460$ nm) actinic excitation, with $\lambda_R = 540$ nm (red in the middle); and in S_1 without actinic excitation under resonance Raman $\lambda_R = 495$ nm (orange in the middle). A shift between the “orange” and “red” spectra reflects differences in S_1 frequencies, as measured from S_0 or S_1 .⁵⁴ Assignments are given in the Supporting Information.⁶²

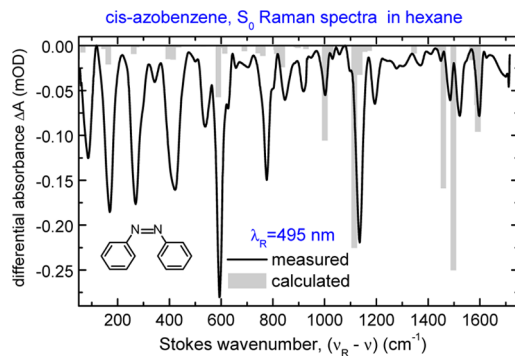


Figure 17. Ground-state (S_0) Raman spectra of *cis*-azobenzene in *n*-hexane from FSR measurements with resonance Raman pumping at $\lambda_R = 495$ nm. Assignments are given in the SI.⁶²

Therefore, we calculated the Raman spectrum for the S_2 state with enforced C_{2h} symmetry, which resulted in one imaginary frequency.

As shown in Figure 16, the calculations mostly capture the main spectral features, at least the C–C, N–C, and N=N stretching modes with small admixtures of the C–C–H bending motions in the higher frequency range above 1000 cm⁻¹. However, the richness of the experimental spectrum of the S_n state may suggest contributions from the other nearby states in addition to the target $\pi\pi^*$ one, which hampers its interpretability. Of interest are the bands at 644 or 657 and 847 or 881 cm⁻¹ that emerge in the spectrum of S_1 . In our calculations, the intense contributions in these regions are associated with bending of the C–N=N angles. The increase in these angles is among the principal changes in S_1 in the course of its relaxation upon vertical excitation from S_0 , and high Raman contributions due to these modes are not surprising.

In *cis*-azobenzene, the agreement of the experimental and the calculated ground-state Raman intensities looks somewhat worse than in the trans conformation. This is mostly due to the high intensity of the bending and deformation modes below 1000 cm⁻¹, an effect that is not paralleled on the trans side. These intense lower frequency vibration are largely associated with the deformations in the central –N=N– bridge that affect the conjugation with the phenyl rings. It turns out that in the nonplanar and sterically strained *cis* conformer the electron density is more readily deformable upon geometric distortions.

4. SUMMARY AND CONCLUSION

4.1. Potential Energy Surface (PES). The excited-state evolution of azobenzene is summarized with the help of Figure 18. Here we draw a potential energy scheme that is consistent with our experiment and calculations. Closed squares mark population (wavepacket) positions upon vertical $n\pi^*(S_1)$ or $\pi\pi^*(S_n)$ excitation, whereas open and closed circles denote stationary points and conical intersections (I). Relaxation (isomerization) paths via the intersections are indicated by dashed arrows, where numbers at the arrows are the corresponding yields. Hula-twist is chosen as an effective reaction coordinate, as was implied by the independence of the isomerization dynamics on viscosity. Real potential surfaces of azobenzene are, of course, multidimensional, and not all important conical intersections can be visualized with the simplified picture in Figure 18.

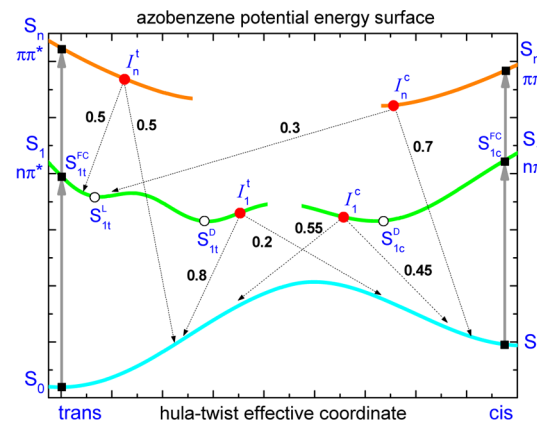


Figure 18. Azobenzene potential energy surface and relaxation/isomerization pathways consistent with our experiment and calculations. Independence of the dynamics on solvent viscosity suggests the hula-twist isomerization coordinate. Closed squares mark wavepacket positions upon vertical $n\pi^*(S_1)$ or $\pi\pi^*(S_n)$ excitation, while open and closed circles denote stationary points and conical intersections (I), respectively. Relaxation/isomerization via the intersections is indicated by dashed arrows marked with yields Y in *n*-hexane. For trans upon $n\pi^*$ excitation, the wavepacket evolves from S_{1t}^{FC} to S_{1t}^L with $\tau_1 = 0.3$ ps, overcomes an 8 kJ/mol barrier to reach a dark intermediate S_{1t}^D with $\tau_2 = 3$ ps, and finally relaxes to S_0 via I_1^L over an 12 kJ/mol barrier with $\tau_3 = 16$ ps. For *cis*-azobenzene upon $n\pi^*$ excitation, population relaxation to S_{1t}^D is barrierless with 0.1 ps; subsequent relaxation to S_0 occurs with 1.1 ps via I_1^L over a 6 kJ/mol barrier. Upon $\pi\pi^*$ excitation of trans, relaxation proceeds via I_n^L with 0.1 ps; 50% population reach S_{1t}^L and 50% experience cascade relaxation $S_n \rightarrow S_1 \rightarrow S_0$ through a different S_1 region, not accessible by the $n\pi^*$ excitation. For *cis* with $\pi\pi^*$ excitation, 30% isomerize to trans via I_n^L resulting in mixed (trans/cis) S_1 population. The other 70% experience cascade relaxation $S_n \rightarrow S_1 \rightarrow S_0$, mainly via an S_1 region not accessible by the $n\pi^*$ excitation. The cis-to-trans barrier in S_0 is 88 kJ/mol.

4.2. $n\pi^*$ Excitation, Intermediates S_{1t}^L , S_{1t}^D , and S_{1c}^D . For *trans*-azobenzene upon $n\pi^*$ excitation, population is created at the Franck–Condon point S_{1t}^{FC} . Relaxation to a local minimum S_{1t}^L occurs with $\tau_1 = 0.3$ ps^{23–25} (in agreement with the fluorescence Stokes shift and decay). Further population relaxation to a dark intermediate S_{1t}^D with $\tau_2 = 3$ ps is relatively slow and suggests a barrier of 8 kJ/mol. The subsequent $S_{1t}^L \rightarrow S_0$ decay with $\tau_3 = 16$ ps occurs via intersection I_1^L over a 12 kJ/mol barrier. In TA spectra, the intermediate S_{1t}^D corresponds to the ESA4 band peaked at 300 nm (Figure 6, Table 1). Previously a similar interpretation of the S_1 trans evolution was proposed by Moore and coworkers.^{20–22}

For *cis*-azobenzene upon $n\pi^*$ excitation, population relaxes first barrierless with $\tau_1 = 0.1$ ps to a dark intermediate S_{1c}^D and then to S_0 via the different intersection I_1^c , with $\tau_2 = 1.1$ ps over a 6 kJ/mol barrier. The barriers imply that the slow relaxation times τ_2 and τ_3 shall be temperature-dependent. Future experiments may check this prediction.

4.3. Isomerization upon $\pi\pi^*$ Excitation. For *trans*-azobenzene, our main result is as follows. One half of the initial S_n population relaxes via intersection I_n^L to the same S_{1t}^L region from which the $n\pi^*$ fluorescence occurs (Figure 18). The other half reaches a different S_1 area, not accessible with $n\pi^*$ excitation. This part of the population reaches S_0 via the cascade relaxation $S_n \rightarrow S_1 \rightarrow S_0$. When assuming that this relaxation results solely in the trans isomer, the full trans-to-cis isomerization yield would be half of that under $n\pi^*$ excitation

(0.2), resulting in the 0.1 yield as actually observed. The result is also consistent with the bleach decay upon $\pi\pi^*$ excitation (Figure 5, Table 1), provided that the fast 1.2 ps component is ascribed to the cascade channel $S_n \rightarrow S_1 \rightarrow S_0$.

For *cis*-azobenzene upon $\pi\pi^*(S_n)$ excitation, 30% of S_n population isomerizes to trans in S_1 via I_n^c intersection (on a 0.1 ps scale), as evidenced by the transient spectra and kinetics. This result is important in two aspects. It demonstrates for the first time isomerization via a higher order (S_n/S_1) conical intersection. Second, it shows how fast the isomerization process can be. Previously we have already seen that the S_1 isomerization of 1,1'-dimethylstilbene⁴⁷ and stiff-stilbene⁴⁸ proceeds with 0.2 to 0.3 ps; here the process takes 0.1 ps or even less time.

4.4. Independence on Viscosity and the Isomerization Paths.

We believe that the hula-twist represents the most probable isomerization path. The inversion mechanism should be excluded because it is inconsistent with the established quasistationary intermediates S_{1t}^D and S_{1c}^D ; as far as we know, no calculations predict such states for the inversion. The torsion pathway should be excluded as well because the isomerization kinetics are independent of solvent viscosity. (In this context, also recall that torsion cannot operate under strong constraints.^{1–4}). At the same time, the hula-twist is in agreement with the independence on viscosity and in addition permits quasistationary intermediate conformations.¹²

In conclusion, we have reexamined the photoisomerization of azobenzene with transient broadband spectroscopies. Comprehensive excited-state *cis* and trans spectra are presented for comparison with quantum-chemical calculations. For the trans-to-*cis* and *cis*-to-trans paths, long-lived S_1 intermediates are tentatively established. Future temperature-dependent measurements could provide a sensitive check for the model. Normalization of the transient spectra to a given population provides relative isomerization yields and allows for precise comparison of different evolutions. Thus, upon $\pi\pi^*$ excitations of trans, 50% of the population relaxes to a different S_1 region not accessible with $n\pi^*$ excitation. For *cis* under $\pi\pi^*$ excitation, 30% of the population isomerizes to trans via S_n/S_1 conical intersection on a 0.1 ps scale. Independence of the reaction kinetics on solvent viscosity and the long-lived S_1 intermediate favors the hula-twist as the most probable isomerization mechanism.

ASSOCIATED CONTENT

Supporting Information

Additional stationary spectra, TA spectra and kinetics, Raman spectra and kinetics, and tables of vibrational wavenumbers. This material is available free of charge via the Internet at <http://pubs.acs.org>.

AUTHOR INFORMATION

Notes

The authors declare no competing financial interest.

ACKNOWLEDGMENTS

We thank the Deutsche Forschungsgemeinschaft for financial support (Er 154/10-3). I.N.I. and A.A.G. are thankful for the computational support by the Supercomputing Center of the Lomonosov Moscow State University.⁶¹

REFERENCES

- Rau, H.; Lueddecke, E. On the Rotation-Inversion Controversy on Photoisomerization of Azobenzenes. Experimental Proof of Inversion. *J. Am. Chem. Soc.* **1982**, *104*, 1616–1620.
- Rau, H.; Shen, Y.-Q. Photoisomerization of Sterically Hindered Azobenzenes. *J. Photochem. Photobiol., A* **1988**, *42*, 321–327.
- Rau, H. Photoisomerization of Benzenes. In *Photoreactive Organic Thin Films*; Academic Press: Boston, 2002.
- Siewertsen, R.; Neumann, H.; Buchheim-Stehn, B.; Herges, R.; Näther, C.; Renth, F.; Temps, F. Highly Efficient Reversible Z-E Photoisomerization of a Bridged Azobenzene with Visible Light through Resolved S_1 ($n\pi^*$) Absorption Bands. *J. Am. Chem. Soc.* **2009**, *131*, 15594–15595.
- Waldeck, D. H. Photoisomerization Dynamics of Stilbenes. *Chem. Rev.* **1991**, *91*, 415–436.
- Pollard, M. M.; Meetsma, A.; Feringa, B. L. A Redesign of Light-Driven Rotary Molecular Motors. *Org. Biomol. Chem.* **2008**, *6*, 507–512.
- Liu, F.; Morokuma, K. Computational Study on the Working Mechanism of a Stilbene Light-Driven Molecular Rotary Motor: Sloped Minimal Energy Path and Unidirectional Nonadiabatic Photoisomerization. *J. Am. Chem. Soc.* **2012**, *134*, 4864–4876.
- Khan, A.; Kaiser, C.; Hecht, S. Prototype of a Photoswitchable Foldamer. *Angew. Chem., Int. Ed.* **2006**, *45*, 1878–1881.
- Bleger, D.; Liebig, T.; Thiermann, R.; Maskos, M.; Rabe, J. P.; Hecht, S. Light-Orchestrated Macromolecular “Accordions”: Reversible Photoinduced Shrinking of Rigid-Rod Polymers. *Angew. Chem., Int. Ed.* **2011**, *50*, 12559–12563.
- Yager, K. G.; C. Barrett, C. J. Novel Photo-Switching Using Azobenzene Functional Materials. *J. Photochem. Photobiol., A* **2006**, *182*, 250–261.
- Böckmann, M.; Doltsinis, N. L.; Marx, D. Enhanced Photoswitching of Bridged Azobenzene Studied by Nonadiabatic *ab Initio* Simulation. *J. Chem. Phys.* **2012**, *137* (22A505), 1–10.
- Böckmann, M.; Doltsinis, N. L.; Marx, D. Nonadiabatic Hybrid Quantum and Molecular Mechanic Simulations of Azobenzene Photoswitching in Bulk Liquid Environment. *J. Phys. Chem. A* **2010**, *114*, 745–754.
- Liu, R. S. H.; Asato, A. E. The Primary Process of Vision and the Structure of Bathorhodopsin: A Mechanism for Photoisomerization of Polyenes. *Proc. Natl. Acad. Sci. U.S.A.* **1985**, *82*, 259–263.
- Liu, R. S. H.; Hammond, G. S. The case of Medium-Dependent Dual Mechanisms for Photoisomerization: One-Bond Flip and Hula-Twist. *Proc. Natl. Acad. Sci. U.S.A.* **2000**, *97*, 11153–11158.
- Ruiz, D. S.; Cembran, A.; Garavelli, M.; Olivucci, M.; Fuß, W. Structure of the Conical Intersections Driving the *cis*-trans Photoisomerization of Conjugated Molecules. *Photochem. Photobiol.* **2002**, *76*, 622–633.
- Yuan, S.; Dou, Y.; Wu, W.; Hu, Y.; Zhao, J. Why Does trans-Azobenzene Have a Smaller Isomerization Yield for $\pi\pi^*$ Excitation than for $n\pi^*$ Excitation. *J. Phys. Chem. A* **2008**, *112*, 13326–13334.
- Jiang, C.-W.; Xie, R.-H.; Li, F.-L.; Allen, R. E. Comparative Studies of the trans-cis Photoisomerizations of Azobenzene and a Bridged Azobenzene. *J. Phys. Chem. A* **2011**, *115*, 244–249.
- Bortolus, P.; Monti, S. Cis-Trans Photoisomerization of Azobenzene. Solvent and Triplet Donors Effects. *J. Phys. Chem.* **1979**, *83*, 648–652.
- Siampiringué, N.; Guyot, G.; Monti, S.; Bortolus, P. The Cis-Trans Photoisomerization of Azobenzene: An Experimental Reexamination. *J. Photochem.* **1987**, *37*, 185–188.
- Lednev, I. K.; Ye, T.-Q.; Hester, R. E.; Moore, J. N. Femtosecond Time-Resolved UV-Visible Absorption Spectroscopy of Trans-Azobenzene in Solution. *J. Phys. Chem.* **1996**, *100*, 13338–13341.
- Lednev, I. K.; Ye, T.-Q.; Matousek, P.; Towrie, M.; Foggi, P.; Neuwahl, F. V. R.; Umapathy, S.; Hester, R. E.; Moore, J. N. Femtosecond Time-Resolved UV-Visible Absorption Spectroscopy of Trans-Azobenzene: Dependence on Excitation Wavelength. *Chem. Phys. Lett.* **1998**, *290*, 68–74.

- (22) Lednev, I. K.; Ye, T.-Q.; Abbott, L. C.; Hester, R. E.; Moore, J. N. Photoisomerization of a Capped Azobenzene in Solution Probed by Ultrafast Time-Resolved Electronic Absorption Spectroscopy. *J. Phys. Chem. A* **1998**, *102*, 9161–9166.
- (23) Nägele, T.; Hoche, R.; Zinth, W.; Wachtveitl, J. Femtosecond Photoisomerization of Cis-Azobenzene. *Chem. Phys. Lett.* **1997**, *272*, 489–495.
- (24) Satzger, H.; Spörlein, S.; Root, C.; Wachtveitl, J.; Zinth, W.; Gilch, P. Fluorescence Spectra of Trans- and Cis-Azobenzene-Emission from the Frank-Condon State. *Chem. Phys. Lett.* **2003**, *372*, 216–223.
- (25) Satzger, H.; Root, C.; Braun, M. Excited-State Dynamics of Trans- and Cis-Azobenzene after UV Excitation in the $\pi\pi^*$ Band. *J. Phys. Chem. A* **2004**, *108*, 6265–6271.
- (26) Azuma, J.; Tamai, N.; Shishido, A.; Ikeda, T. Femtosecond Dynamics and Stimulated Emission from the S_2 State of a Liquid Crystalline Trans-Azobenzene. *Chem. Phys. Lett.* **1998**, *288*, 77–82.
- (27) Fujino, T.; Tahara, T. Picosecond Time-Resolved Raman Study of trans-Azobenzene. *J. Phys. Chem. A* **2000**, *104*, 4203–4210.
- (28) Fujino, T.; Arzhantsev, S. Yu.; Tahara, T. Femtosecond Time-Resolved Fluorescence Study of Photoisomerization of Trans-Azobenzene. *J. Phys. Chem. A* **2001**, *105*, 8123–8129.
- (29) Schultz, T.; Quenneville, J.; Levine, B.; Toniolo, A.; Martinez, T. J.; Lochbrunner, S.; Schmitt, M.; Shaffer, J. P.; Zgierski, M. Z.; Stolow, A. Mechanism and Dynamics of Azobenzene Photoisomerization. *J. Am. Chem. Soc.* **2003**, *125*, 8098–8099.
- (30) Pancur, T.; Renth, F.; Temps, T.; Harbaum, B.; Krüger, A.; Herges, R.; Näther, C. Femtosecond Fluorescence up-Conversion Spectroscopy of a Rotation-Restricted Azobenzene after Excitation to the S_1 State. *Phys. Chem. Chem. Phys.* **2005**, *7*, 1985–1989.
- (31) Chang, C.-W.; Lu, Y.-C.; Wang, T.-T.; Diau, E. W.-G. Photoisomerization Dynamics of Azobenzene in Solution with S_1 Excitation: A Femtosecond Fluorescence Anisotropy Study. *J. Am. Chem. Soc.* **2004**, *126*, 10109–10118.
- (32) Bandara, H. M. D.; Burdette, S. C. Photoisomerization in Different Classes of Azobenzene. *Chem. Soc. Rev.* **2012**, *41*, 1809–1825.
- (33) Fliegl, H.; Köhn, A.; Hättig, C.; Ahlrichs, R. Ab Initio Calculation of the Vibrational and Electronic Spectra of trans- and cis-Azobenzene. *J. Am. Chem. Soc.* **2003**, *125*, 9821–9827.
- (34) Diau, E. W.-G. A new Trans-to-Cis Photoisomerization Mechanism of Azobenzene on the S_1 Surface. *J. Phys. Chem. A* **2004**, *108*, 950–956.
- (35) Crecca, C. R.; Roitberg, A. E. Theoretical Study of the Isomerization Mechanism of Azobenzene and Disubstituted Azobenzene Derivatives. *J. Phys. Chem. A* **2006**, *110*, 8188–8203.
- (36) Granucci, G.; Persico, M. Excited State Dynamics with the Direct Trajectory Surface Hopping Method: Azobenzene and its Derivatives as a case Study. *Theor. Chem. Acc.* **2007**, *117*, 1131–1143.
- (37) Cembran, A.; Bernardi, F.; Garavelli, M.; Gagliardi, L.; Orlandi, G. On the Mechanism of the cis-trans Isomerization in the Lowest Electronic States of Azobenzene: S_0 , S_1 , and T_1 . *J. Am. Chem. Soc.* **2004**, *126*, 3234–3243.
- (38) Conti, I.; Garavelli, M.; Orlandi, G. The Different Photoisomerization Efficiency of Azobenzene in the Lowest $n\pi^*$ and $\pi\pi^*$ Singlets: The Role of a Phantom State. *J. Am. Chem. Soc.* **2008**, *130*, 5216–5230.
- (39) Nonnenberg, C.; Gaub, H.; Frank, I. First-principles Simulation of the Photoreaction of a Capped Azobenzene: the Rotational Pathway is Feasible. *ChemPhysChem* **2006**, *7*, 1455–1461.
- (40) Harabuchi, Y.; Ishii, M.; Nakayama, F.; Noro, T.; Taketsugu, T. A multireference Perturbation Study of the NN Stretching Frequency of trans-Azobenzene in $n\pi^*$ Excitation and an Implication for the Photoisomerization Mechanism. *J. Chem. Phys.* **2013**, *138*, 064305.
- (41) Kovalenko, S. A.; Dobryakov, A. L.; Ruthmann, J.; Ernstsing, N. P. Femtosecond Spectroscopy of Condensed Phases with Chirped Supercontinuum Probing. *Phys. Rev. A* **1999**, *59*, 2369–2384.
- (42) Dobryakov, A. L.; Kovalenko, S. A.; Weigel, A.; Perez-Lustres, J. L.; Lange, J.; Müller, A.; Ernstsing, N. P. *Rev. Sci. Instrum.* **2010**, *81*, 113106.
- (43) Kovalenko, S. A.; Schanz, R.; Hennig, H.; Ernstsing, N. P. Cooling Dynamics of an Optically Excited Molecular Probe in Solution from Femtosecond Broadband Transient Absorption Spectroscopy. *J. Chem. Phys.* **2001**, *115*, 3256–3273.
- (44) Perez-Lustres, J. L.; Rodriguez-Prieto, F.; Mosquera, M.; Senyushkina, T. A.; Ernstsing, N. P.; Kovalenko, S. A. Ultrafast Proton Transfer to Solvent: Molecularity and Intermediates from Solvation- and Diffusion-Controlled Regimes. *J. Am. Chem. Soc.* **2007**, *129*, 5408–5418.
- (45) Karunakaran, V.; Kleinermanns, K.; Imrota, R.; Kovalenko, S. A. Photoinduced Dynamics of Guanosine Monophosphate in Water from Broad-Band Transient Absorption Spectroscopy and Quantum-Chemical Calculations. *J. Am. Chem. Soc.* **2009**, *131*, 5839–5850.
- (46) Kovalenko, S. A.; Dobryakov, A. L.; Ioffe, I.; Ernstsing, N. P. Evidence for the Phantom State in photoinduced cis-trans Isomerization of Stilbene. *Chem. Phys. Lett.* **2010**, *493*, 255–258.
- (47) Berndt, F.; Dobryakov, A. L.; Quick, M.; Mahrwald, R.; Ernstsing, N. P.; Lenoir, D.; Kovalenko, S. A. Long-Lived Perpendicular Conformation in the Photoisomerization Path of 1,1'-Dimethylstilbene and 1,1'-Diethylstilbene. *Chem. Phys. Lett.* **2012**, *544*, 39–42.
- (48) Quick, M.; Berndt, F.; Dobryakov, A. L.; Ioffe, I. N.; Granovsky, A. A.; Knie, C.; Mahrwald, R.; Lenoir, D.; Ernstsing, N. P.; Kovalenko, S. A. Photoisomerization Dynamics of Stiff-Stilbene in Solution. *J. Phys. Chem. B* **2014**, *118*, 1389–1402.
- (49) (a) Schanz, R.; Kovalenko, S. A.; Kharlanov, V.; Ernstsing, N. P. Broad-Band Fluorescence Upconversion for Femtosecond Spectroscopy. *Appl. Phys. Lett.* **2001**, *79*, 566–568. (b) Kovalenko, S. A.; Schanz, R.; Senyushkina, T. A.; Ernstsing, N. P. Femtosecond Spectroscopy of *p*-Dimethylaminocyanostilbene in Solution – no evidence for dual fluorescence. *Phys. Chem. Chem. Phys.* **2002**, *4*, 703–707.
- (50) (a) Zhao, L.; Lustres, J. L. P.; Farztdinov, V.; Ernstsing, N. P. Femtosecond Fluorescence Spectroscopy by Upconversion with Tilted Gate Pulses. *Phys. Chem. Chem. Phys.* **2005**, *7*, 1716–1725. (b) Sajadi, M.; Quick, M.; Ernstsing, N. P. Femtosecond Broadband Fluorescence Spectroscopy by Down- and Up-Conversion in BBO Crystals. *Appl. Phys. Lett.* **2013**, *103*, 173514.
- (51) Zhang, X.-X.; Würth, C.; Zhao, L.; Resch-Genger, U.; Ernstsing, N. P.; Sajadi, M. Femtosecond Broadband Fluorescence Upconversion Spectroscopy: Improved Setup and Photometric Correction. *Rev. Sci. Instrum.* **2011**, *82* (063108), 1–8.
- (52) Kovalenko, S. A.; Dobryakov, A. L.; Ernstsing, N. P. An Efficient Setup for Femtosecond Stimulated Raman Spectroscopy. *Rev. Sci. Instrum.* **2011**, *82* (063102), 1–10.
- (53) Dobryakov, A. L.; Ioffe, I.; Granovsky, A. A.; Ernstsing, N. P.; Kovalenko, S. A. Femtosecond Raman Spectra of cis-Stilbene and trans-Stilbene with Isotopomers in Solution. *J. Chem. Phys.* **2012**, *137* (244505), 1–16.
- (54) Dobryakov, A. L.; Quick, M.; Ioffe, I.; Granovsky, A. A.; Ernstsing, N. P.; Kovalenko, S. A. Excited-State Raman Spectroscopy with and without Actinic Excitation: S_1 Raman Spectra of trans-Azobenzene. *J. Chem. Phys.* **2014**, *140* (184310), 1–5.
- (55) Granovsky, A. A. Extended Multi-Configuration Quasi-Degenerate Perturbation Theory: The New Approach to Multi-State Multi-Reference Perturbation Theory. *J. Chem. Phys.* **2011**, *134*, 214113.
- (56) Granovsky, A. A. *Firefly*, version 8.1.0. <http://classic.chem.msu.su/gran/firefly/index.html>.
- (57) Schmidt, M. W.; Baldridge, K. K.; Boatz, J. A.; Elbert, S. T.; Gordon, M. S.; Jensen, J. H.; Koseki, S.; Matsunaga, N.; Nguyen, K. A.; Su, S.; Windus, T. L.; Dupuis, M.; Montgomery, J. A. General Atomic and Molecular Electronic Structure System. *J. Comput. Chem.* **1993**, *14*, 1347–1363.
- (58) Laikov, D. N. Fast Evaluation of Density Functional Exchange-Correlation Terms Using the Expansion of the Electron Density in Auxiliary Basis Sets. *Chem. Phys. Lett.* **1997**, *281*, 151–156.

- (59) Perdew, J. P.; Burke, K.; Ernzerhof, M. Generalized Gradient Approximation Made Simple. *Phys. Rev. Lett.* **1996**, *77*, 3865–3868.
- (60) Ioffe, I. N.; Granovsky, A. A. Photoisomerization of Stilbene: The Detailed XMCQDPT2 Treatment. *J. Chem. Theory Comput.* **2013**, *9*, 4973–4990.
- (61) Sadovnichy, V.; Tikhonravov, A.; Voevodin, V.; Opanasenko, A. In *Contemporary High Performance Computing*; CRC Press: Boca Raton, FL, 2013; pp 283–307.
- (62) Supporting Information to this paper.